RNA helicase DDX5 enables STAT1 mRNA translation and interferon signaling in hepatitis B virus replicating hepatocytes

Jiazeng Sun, Guanhui Wu, Florentin Pastor, Naimur Rahman, Wen-Hung Wang, Zhengtao Zhang, Philippe Merle, Lijian Hui, Anna Salvetti, David Durantel, et al.

RNA helicase DDX5 enables STAT1 mRNA translation and interferon signaling in hepatitis B virus replicating hepatocytes.

Jiazeng Sun[1,2], Guanhui Wu[2,3#], Florentin Pastor[4#], Naimur Rahman[1,2], Wen-Hung Wang[5], Zhengtao Zhang[6], Philippe Merle[7], Lijian Hui[6], Anna Salvetti[4], David Durantel[4], Danzhou Yang[2,3], and Ourania Andrisani[1,2*]

[1]Department of Basic Medical Sciences, [2]Purdue Center for Cancer Research, [3]Department of Medicinal Chemistry and Molecular Pharmacology, and [4] INSERM U1111-CNRS UMR5308 International Center for Infectiology Research (CIRI), [5]Gene Editing Core, Bindley Biosciences Center, Purdue University, West Lafayette, IN 47907. [6]Shanghai Institute of Biochemistry and Cell Biology, Chinese Academy of Sciences, Suzhou, Jiangsu 215121, China. [7]Department of Hepatology, Hôpital de la Croix-Rousse, Hospices Civils de Lyon, Université Lyon 1, Lyon, France

#equal contribution

*corresponding author: andrisao@purdue.edu

Department of Basic Medical Sciences,
Purdue University
201 S. University Street
West Lafayette, IN 47907-2064
Phone: 765-494-8131

Keywords: RNA helicase DEAD box protein 5 (DDX5), STAT1, G-quadruplex, Interferon Signaling, Hepatitis B Virus, Hepatocellular Carcinoma

Conflict of Interest: Nothing to disclose/No conflict

Financial support: This work was supported by NIH grants DK044533 to OA and CA177585 to DY. Shared Resources (Genomics and Bioinformatics Facilities) supported by NIH grant P30CA023168 to Purdue Center for Cancer Research, and NIH/NCRR RR025761.

Word count: 5,045 words excluding references and figure legends; Figures: 10

ABSTRACT

***Objective*:** RNA helicase DDX5 is downregulated during hepatitis B virus (HBV) replication, and poor prognosis HBV-related hepatocellular carcinoma (HCC). The objective of this study is to investigate the role of DDX5 in interferon signaling. We provide evidence of a novel mechanism involving DDX5 that enables translation of transcription factor STAT1 mediating the interferon (IFN) response.

Design and Results*:** Molecular, pharmacologic, and biophysical assays were used together with cellular models of HBV replication, HCC cell lines, and liver tumors. We demonstrate that DDX5 regulates STAT1 mRNA translation by resolving a G-quadruplex (rG4) RNA structure, proximal to the 5' end of STAT1 5'UTR. We employed luciferase reporter assays comparing wild type (WT) *vs*. mutant (MT) rG4 sequence, rG4-stabilizing compounds, CRISPR/Cas9 editing of the STAT1-rG4 sequence, and circular dichroism determination of the rG4 structure. STAT1-rG4 edited cell lines were resistant to the effect of rG4-stabilizing compounds in response to IFN-α, while HCC cell lines expressing low DDX5 exhibited reduced interferon response. Ribonucleoprotein and electrophoretic mobility assays demonstrated direct and selective binding of RNA helicase-active DDX5 to the WT STAT1-rG4 sequence. Immunohistochemistry of normal liver and liver tumors demonstrated that absence of DDX5 corresponded to absence of STAT1. Significantly, knockdown of DDX5 in HBV infected HepaRG cells reduced the anti-viral effect of IFN-α. ***Conclusion: RNA helicase DDX5 resolves a G-quadruplex structure in 5'UTR of STAT1 mRNA, enabling STAT1 translation. We propose that DDX5 is a key regulator of the dynamic range of interferon response during innate immunity and adjuvant IFN-α therapy.

Introduction

Interferon Type I/III signaling acting through the JAK/STAT pathway exerts antiviral, anti-tumor, and immunomodulatory effects (1, 2). Effects of IFN-α and IFN-β are mediated by tyrosine phosphorylation of transcription factors STAT1 and STAT2, followed by formation of ISGF3 complex via interaction with IRF9, translocation to the nucleus, and transcriptional induction of Interferon Stimulated Genes (ISGs). In addition to tyrosine phosphorylation, STAT1 activity is further modulated by modifications including methylation (3), acetylation (4) and ubiquitination (5). Since STAT1 is involved in all types (I/III) of interferon signaling (6), these post-translational modifications influence all types (I/III) of interferon signaling, depending on cellular context. Herein, we provide evidence for a novel mechanism of STAT1 regulation, involving translational control of STAT1 mRNA, studied in the HBV replicating HepAD38 cell line (7) and HBV infection model of differentiated HepaRG cells (8).

Hepatitis B virus (HBV) infection is a significant global health problem with more than 250 million chronically infected patients. Chronic HBV infection is associated with progressive liver disease, cirrhosis, and development of hepatocellular carcinoma (HCC). Curative treatments for early stage HCC include liver resection, transplantation, or local ablation. In advanced stage HCC, multi-kinase inhibitors (9-11), offer only palliative benefits. In addition, because IFNs exert both antiviral and anti-proliferative effects (12, 13), adjuvant IFN-α therapy has been extensively applied for treatment of chronically HBV-infected patients with HCC. Unfortunately, many patients do not respond to IFN-α (14). Importantly, HCC patients with increased expression of the ISG IFIT3, a direct transcription target of STAT1 (15), predict positive response to IFN-α therapy (16), suggesting IFN-α non-responders lack STAT1 activation and/or expression.

Viruses have evolved effective strategies to hijack cellular pathways for their growth advantage, including mechanisms for immune evasion. In our studies, we have identified a cellular mechanism hijacked by HBV associated with both viral biosynthesis and poor prognosis HBV-related HCC (17-19). This mechanism involves the chromatin modifying PRC2 complex and RNA helicase DDX5. PRC2 mediates repressive histone modifications (H3K27me3)(20), while RNA helicase DDX5 is involved in transcription, epigenetic regulation, miRNA processing, mRNA splicing, decay, and translation (21, 22). Interestingly, HBV infection downregulates DDX5 via induction of two microRNA clusters (23), miR17~92 and miR106~25 (17-19). Moreover, HBV replicating cells with reduced DDX5 exhibit Wnt activation, resistance to chemotherapeutic agents (23), and reduced protein levels of STAT1, as we describe herein.

In this study, we provide evidence that DDX5 is involved in a novel mechanism of translational control of STAT1, a transcription factor mediating all types (I/III) of interferon signaling. Specifically, RNA helicase DDX5 resolves a secondary RNA structure called G-quadruplex (24), located in the 5' untranslated region (5'UTR) of STAT1 mRNA, thereby enabling its translation. G-quadruplexes are four-stranded structures formed in guanine (G)-rich sequences (25), and when located in 5'UTRs of mRNAs, influence post-transcriptional regulation of gene expression (20). One of the first examples of translational repression by an RNA G-quadruplex (rG4) was demonstrated for human NRAS mRNA (26). Bioinformatics analysis estimated nearly 3,000 5'UTR rG4s in the human genome (26), and rG4-sequencing of polyA+ HeLa RNA generated a global map of thousands rG4 structures (27). Recently, it was discovered that DDX5 proficiently resolves both RNA and DNA G4 structures (28).

The significance of this mechanism of translational control of STAT1 is dependence on the protein level and activity of the rG4-resolving helicase. Our results presented herein demonstrate

that the interferon response is influenced by this dynamic mechanism of STAT1 translational regulation, dependent on the protein level of DDX5.

Materials and Methods

Cell culture: Human hepatocellular carcinoma (HCC) cell lines HepG2, Huh7, Snu387, Snu423, HepaRG (29), HepAD38 (7), CLC15 and CLC46 (30) were grown as described, and regularly tested for mycoplasma using PCR Mycoplasma Detection Kit (Abm). HepAD38 cells support HBV replication by tetracycline removal (7). HepAD38 were STR tested by ATCC. Human A549 and Panc-1 cells were grown in DMEM with 10% FBS. Stable HepaRG cell lines were constructed expressing DDX5-FLAG-WT, and site directed DDX5-FLAG mutants K144N and D248N described previously (18), using the doxycycline inducible vector PLVX-puro (Supporting Table S1).

Transfection assays: HepAD38, Huh7, and HepaRG cells ($0.3x10^6$ cells per well of 6-well plate) were transfected with control (Ctrl) or DDX5 siRNAs (40 nM). Following transfection (48 h), cells were harvested for RNA or protein extraction and analyzed by qRT-PCR or immunoblotting, respectively. HepAD38, Huh7, and HepaRG cells ($0.1x10^6$ cells per well of 12-well plate) were co-transfected with Renilla luciferase (25 ng) and WT STAT1-5'UTR-Luciferase (pFL-SV40-STAT1-5'UTR a gift from Dr. Ming-Chih Lai) (50 ng) or mutant MT-STAT1-5'UTR-Luciferase (50 ng) using Lipofectamine 3000 (Life Technologies). In HepAD38 cells, HBV replication was induced by tetracycline removal 4 days prior to transfection with Renilla and Firefly luciferase vectors. Ctrl or DDX5 siRNAs (40 nM each) were co-transfected with Renilla and Firefly luciferase vectors using RNAiMax (Life Technologies). Plasmids used are listed in Supporting

Table S1. Firefly luciferase activity was measured 24 h after transfection using Dual Luciferase Assay system (Promega) according to manufacturer's protocol, normalized to Renilla luciferase.

HBV infection assays. HepaRG cells plated in 24-well plates were subjected to DMSO-induced differentiation for one month (31). dHepaRG cells were infected with HBV at multiplicity of infection (moi) = 500, in the presence of 4% Peg8000. One day post-infection, cells were washed with phosphate buffered saline (PBS) and maintained in culture until establishment of infection i.e., stable cccDNA level at 5-7 days. siRNAs (25 nM) were transfected on day 8 post-infection (p.i) with lipofectamine RNAimax, according to supplier's recommendations. IFNα treatments were performed, starting on day 11 p.i., every 3 days. Cells were harvested on day 17 p.i., to quantify viremia (qPCR) and viral RNAs by RT-qPCR.

RNA preparation and qRT-PCR assay: RNA preparation and qRT-PCR performed according to manufacturer's instructions, employing commercially available kits (Supporting Table S2). Primer sequences listed in Supporting Table S3.

Immunoblot and Immunohistochemistry assays performed as described (18). Densitometric analysis of immunoblots was by ImageJ. Antibodies used are listed in Supporting Table S4.

Circular Dichroism spectroscopy of RNA oligonucleotides performed as described (32), employing Jasco J-1100 spectropolarimeter equipped with thermoelectrically controlled cell holder. CD measurements were performed using quartz cell with optical path length of 1 mm. Blank sample contained only buffer (25 mM Tris-HCl, pH 7.4). Each CD spectroscopy measurement was the average of two scans, collected between 340 and 200 nm at 25°C, scanning speed 50 nm/min. CD melting experiments were performed at 264 nm with heating rate of 2°C/min between 25°C and 95°C. RNA sample concentration was 10 μM.

CRISPR/Cas9 gene editing: Huh7 and HepaRG cells were used to introduce indels targeting essential nucleotides of the G-quadruplex structure in 5' UTR region of DDX5 gene (33). Ribonucleoprotein (RNP) of Cas9-2NLS (10 pmol) and guide RNA (50 pmol, Synthego) were loaded onto a 10 µl Neon Tip, and electroporated into $1x10^5$ Huh7 and HepaRG cells, using Neon Transfection System at 1200 V, for 20 msec and 4 pulses (ThermoFisher Scientific), according to manufacturer's instructions. Genomic DNA was isolated and used for rapid PAGE genotyping (34) to validate incorporation of indels, 48 h after electroporation. Validated pools of cells were subjected to clonal selection. Isolated single colonies were confirmed by rapid PAGE genotyping and allelic sequencing.

Ribonucleoprotein Immunoprecipitation (RIP) Assay: RIP assays employed the Magna RIP™ RNA-Binding Protein Immunoprecipitation Kit (Millipore Sigma) following manufacturer's instructions. Primer sequences and antibodies used are listed in Supporting Table S3 and S4, respectively.

RNA pull down assay: RNA folding and pull down assays were performed as described with modifications (35). Briefly, synthetic 5'-biotinylated rG4 (Bio-rG4) and rG4mut (Bio-rG4mut) RNA oligonucleotides (Millipore Sigma) were diluted to 5 mM in folding buffer, heated to 95 °C, and cooled to 25°C. G-quadruplex formation determined by circular dichroism (CD). Whole cell extracts from HepAD38, Huh7, and HepaRG cells were incubated with folded biotinylated RNAs (Table S3), followed by pull down with streptavidin beads (Promega). Bound proteins analyzed by immunoblotting.

Electrophoretic Mobility Shift Assay (EMSA): DDX5-FLAG-WT, DDX5-FLAG-K144N and DDX5-FLAG-D248N proteins were purified from lysates of respective HepaRG cell lines

following doxycycline induction (48 h), using Anti-FLAG M2 Magnetic Beads (Millipore Sigma) per manufacturer's instructions. Synthetic Bio-rG4 (500 nM) or Bio-rG4mut (500 nM) RNA oligonucleotides (Millipore Sigma) were processed to form G-quadruplex as described, and incubated with increasing amount (1-100 ng/µl) of DDX5 protein in reactions containing 50 mM Tris-HCl, pH 9.0, 50 mM KCl, 1 mM $MgCl_2$, 0.5 mM DTT and 100 µg/ml BSA, on ice for 15 min. Binding reactions were adjusted to 5% (v/v) with glycerol and analyzed by electrophoresis on a 1.5% native agarose minigel in cold 0.5X Tris-Borate-EDTA buffer, pH 9.0. RNA oligonucleotides were stained by SYBR™-Gold dye (ThermoFisher) and visualized by ChemiDoc™ Touch Imaging System.

Statistical Analysis: Statistical analysis was performed using unpaired *t* test in GraphPad Prism version 6.0 (GraphPad Software, San Diego, CA). Differences were considered significant when $p < 0.05$.

Results

We examined various liver cancer cell lines, HepG2, Huh7, Snu423 and HepaRG for IFN-α response, employing immunoblots for activated phospho-STAT1 (T701) and expression of ISG IRF9. All cell lines responded to IFN-α, including the HBV replicating HepAD38 cell line that contains a stably integrated copy of the HBV genome under control of the Tet-off promoter (7) (Fig. 1A and Supplementary Fig. S1A-B). In the absence of IFN-α treatment, HBV replication in HepAD38 cells exerted a small but reproducible reduction on STAT1 protein level (Fig. 1A). Following IFN-α treatment for 24 h, levels of STAT1, p-STAT1, and downstream ISGs IRF9 and IFITM3 were similarly reduced (Fig. 1A). Likewise, HBV replication exerted a reproducible

decrease in protein level of DDX5, irrespective of IFN-α treatment (Fig. 1A), as reported previously (18).

To determine whether DDX5 downregulation was associated with downregulation of STAT1 observed during HBV replication (Fig. 1A), we transfected siRNA for DDX5 in HepAD38 cells. Surprisingly, reduction in DDX5 protein resulted in reduction in STAT1 protein level (Fig. 1B). DDX5 knockdown in Huh7 and HepaRG cell lines also resulted in reduced STAT1 protein (Fig. 1B), whose t1/2 was quantified to be 16 h (Supplementary Fig. S2A-B). Next, we examined STAT1 protein levels in three clonal DDX5-knockdown ($DDX5^{KD}$) cell lines, KD2, KD3 and KD5, constructed in HepAD38 cells (23). These cell lines lacked STAT1 protein (Fig. 1C) and IFN-α response (Fig. S2C). Interestingly, STAT1 mRNA levels were unaffected in HBV replicating HepAD38 cells (Fig. 1D), in $DDX5^{KD}$ HepAD38 cells (Fig. 1E), and upon transient siRNA-mediated DDX5 knockdown in HepAD38, Huh7, and HepaRG cells (Fig. 1F), thereby excluding DDX5 effects on STAT1 transcription. By contrast, transfection of STAT1 siRNA abolished STAT1 mRNA detected by qRT PCR, in both WT and $DDX5^{KD}$ HepAD38 cells (Fig. 1E).

The STAT1 gene contains 24 introns. Accordingly, we examined whether intron detention or aberrant splicing are regulated by DDX5. qRT-PCR and RNA-seq intron data analyses of STAT1 in WT HepAD38 cells *vs*. DDX5-knockdown cells excluded STAT1 intron detention (Supplementary Fig. S3A). Likewise, comparison of STAT1 mRNA sequence from WT *vs.* $DDX5^{KD}$ cells, excluded aberrant splicing involving the mRNA splice site in proximity to AUG (Supplementary Fig. S3B). These results suggested DDX5 regulates STAT1 mRNA translation.

rG4 structures in 5'UTR of human STAT1 mRNA

Having excluded DDX5 effects on STAT1 mRNA transcription and processing, we reasoned, the information for post-transcriptional regulation must be located in the sequence or structure of STAT1 5' UTR. Surprisingly, the rG4-seq transcriptomic studies by Kwok et al (27) identified the 5'UTR of human STAT1 mRNA as a high probability mRNA harboring rG4 structures (Supplementary Fig. S3C). To test this hypothesis, and using NRAS as our positive control (26), we examined the effect of several G4 stabilizing compounds (Fig. 2A), including PhenDC3 and RR82 (24), on STAT1 protein level. Both compounds reduced STAT1 and NRAS protein level, without affecting DDX5 protein levels (Fig. 2A) or STAT1 mRNA (Fig. 2B). Similarly, we tested the effect of the G4-interactive TMPyP4 and its corresponding non-G4-interactive TMPyP2 compound (36) on STAT1 protein and mRNA levels, using HepAD38 and Huh7 cells (Fig. 2C). The G4-interactive TMPyP4, similar to RR82, suppressed STAT1 protein levels, whereas the non-G4 interactive TMPyP2 exerted no effect. Importantly, these compounds did not affect DDX5 protein or STAT1 mRNA levels (Fig. 2C). We interpret these results to mean the 5'UTR of STAT1 contains a putative rG4 structure, regulating STAT1 expression post-transcriptionally.

Employing an expression vector driven by the SV40 promoter, we cloned nucleotides (nt) + 1 to +400 of the 5'UTR of STAT1 upstream of Firefly (F.) luciferase gene. This 5'UTR region contains three putative rG4s, labeled as rG4-1, rG4-2 and rG4-3 (Supplementary Fig. S3C). Importantly, rG4-1 is located 30 nt downstream from the start of the 5'UTR. Earlier studies demonstrated rG4s situated proximal or within the first 50 nt to the 5' end of the 5'UTR are functional and effective in repressing translation (37). Based on this reasoning, we focused our analysis on rG4-1 and constructed a mutant (MT) rG4-1 (Fig. 3A), with G to A substitutions within the putative rG4-1 sequence. Transfection in HepAD38 cells of expression vectors containing WT and MT rG4-1 demonstrated a statistically significant increased F. luciferase activity from MT

rG4-1 in comparison to WT rG4-1 vector, while no changes were observed at the mRNA level, both in HepAD38 and Huh7 cells (Fig. 3B). Mutational analyses of rG4-2 and rG4-3 sequences excluded a similar role on STAT1 expression (Supplementary Fig. S4A and B). Next, we examined the effect of HBV replication, using HepAD38 cells, on F. luciferase activity expressed from WT and MT rG4-1 vectors. HBV replication reduced F. luciferase activity only from the WT rG4-1 containing vector, without an effect on F. luciferase mRNA expression (Fig. 3C). Similar results were observed by siRNA knockdown of DDX5 (siDDX5) (Fig. 3C). Employing these expression vectors, we also tested the effect of the G4-stabilizing compounds RR82 and TMPyP4. Both drugs reduced expression only from the WT rG4-1 vector, without an effect on mRNA levels of F. luciferase, tested in HepAD38 (Fig. 3D) and Huh7 (Fig. 3C) cells. Taken together, these results identify the rG4-1 sequence as a functional element in 5'UTR of STAT1 mRNA, regulating its translation.

Genomic editing of rG4-1 increases STAT1 protein levels

Using clustered regularly interspaced short palindromic repeats (CRISPR)/Cas9 technology (38) we edited the genomic rG4-1 sequence of STAT1 in Huh7 and HepaRG cell lines. Several clones were isolated and sequenced, and protein and mRNA levels of STAT1 were determined (Fig. 4 and Supplementary Fig. S5). DNA sequencing of HepaRG clones C5 and C9 (Supplementary Fig. S5) demonstrated C5 cells contain rG4-1 deletions in both alleles, while C9 cells have rG4 changes only in one allele (Fig. 4B). All clones analyzed from Huh7 and HepaRG cells exhibited statistically significant and reproducible increases in protein level of STAT1 in comparison to WT (unedited) cells, while STAT1 mRNA levels remained unchanged (Fig. 4). These results are also supported by luciferase reporter assays containing the edited rG4-1 sequences (Supplementary Fig. S6).

Interestingly, DDX5 knockdown by transfection of DDX5 siRNA had no effect on STAT1 protein levels of clone C5, containing edited rG4 sequence on both STAT1 alleles (Fig. 5A). By contrast, siDDX5 reduced STAT1 protein levels in WT and C9 cells (Fig. 5A). Likewise, STAT1 protein levels of clone C5 were resistant to G4-stabilizing drugs RR82 and TMPyP4, while these compounds reduced STAT1 levels in both WT and C9 cells (Fig. 5B). Next, we examined the interferon response of WT, C5, and C9 cells as a function of co-treatment with RR82 (Fig. 5C). In contrast to WT and C9 cells, the IFN-α response of C5 cells was not inhibited by RR82, in terms of STAT1 protein level and activation, as well as induction of IRF9 and IFITM3 (Fig. 5C and Fig. S7). These results support that both alleles of clone C5 contain nonfunctional rG4-1 structures in 5'UTR of STAT1 mRNA.

The rG4-1 sequence of STAT1 forms G-quadruplex *in vitro.*

To directly determine whether the rG4-1 sequence in 5'UTR of STAT1 indeed forms a G-quadruplex structure, we employed CD spectroscopy, a method that enables study of nucleic acid secondary structure (32, 39). RNA oligonucleotides were synthesized (Fig. 6A) that corresponded to the indicated sequences of rG4-1 found in WT STAT1 mRNA, and in each allele of clones C5 and C9. Since G4 oligonucleotides can form higher-order structures, we included U-streches at the 5' and 3' of the indicated RNA oligonucleotides, and confirmed these RNA molecules were in monomeric form, employing native PAGE (Supplementary Fig. S8). The CD spectrum and thermal stability of these RNA oligonucleotides were studied as a function of K+ addition (100 mM), a cation that stabilizes G4 structures (40). The melting temperature (Tm) of each RNA oligonucleotide is shown (Fig. 6D). Addition of 100 mM KCl increased the Tm of the WT, C9-1, and C9-2 RNA oligonucleotides, supporting formation of stable rG4 structures. By contrast, oligonucleotide C5-1 and C5-2 exhibited no or very small Tm increase in comparison to WT.

These results indicate, the WT, C9-1 and C9-2 sequences form stable rG4 structures, whereas C5-1 and C5-2 lack formation of this structure. These biophysical results are congruent with our biological data, and demonstrate the role of rG4-1 structure in STAT1 translational control.

DDX5 selectively binds STAT1 mRNA with WT rG4-1

To determine whether DDX5 interacts directly with STAT1 mRNA, we performed ribonucleoprotein immunoprecipitation (RIP) assays employing DDX5 antibody, and IgG as negative control. In HepAD38 and Huh7 cells endogenous, immunoprecipitated DDX5 was found in association with STAT1 mRNA, while IgG did not exhibit such association (Fig. 7A). Next, we performed RIP assays in HepaRG cells, WT and clones C5 and C9. Interestingly, endogenous DDX5 associated with STAT1 mRNA in WT and clone C9 cells, while STAT1 mRNA expressed in clone C5, containing mutated rG4-1 sequence on both alleles, lacked binding to DDX5 (Fig. 7B).

To determine whether the enzymatic RNA helicase activity of DDX5 is required for resolving the rG4 STAT1 mRNA structure, we compared the STAT1 mRNA binding potential of WT DDX5 and two mutant forms of DDX5. Mutant DDX5-K144N lacks ATPase activity (41) and DDX5-D248N binds RNA but does not remodel it (18). Employing the HepaRG cell lines expressing the WT and indicated DDX5 mutants, we performed RIP assays (Fig. 7C). DDX5-K144N exhibited significantly reduced binding to endogenous STAT1 mRNA, in comparison to WT and DDX5- D248N (Fig. 7C), supporting the requirement of ATP hydrolysis for STAT1 mRNA binding.

To further confirm that DDX5 binds the rG4-1 sequence, biotinylated oligonucleotides containing WT or mutant rG4-1 (Fig. 8A) were incubated in 100 mM K+ that stabilizes the G4

structure or 100 mM Li+ that does not (40). Mutant rG4-1 does not form stable G4 structure even in the presence of 100 mM K+, determined by CD spectroscopy (Supplementary Fig. S9A). Next, pre-folded RNA oligonucleotides incubated with lysates from HepAD38, Huh7, and HepaRG cells were bound to streptavidin beads, and the retained proteins analyzed by DDX5 immunoblots. Indeed, these pull-down assays show DDX5 selectively binds the WT rG4-1, whose structure is stabilized by 100 mM K+ (Fig. 8A). We also employed the pull-down using the biotinylated WT and MT rG4-1 RNA oligonucleotides to confirm the requirement of the RNA helicase activity in this process. Indeed, both the WT and DDX5-D248N proteins, expressed in HepaRG cells, exhibited enhanced and selective binding to the WT rG4-1 RNA oligo in comparison to the inactive DDX5-K144N (Fig. 8B).

Lastly, to directly demonstrate that DDX5 forms an RNA-protein complex with the WT rG4-1 RNA oligonucleotide, we performed EMSAs using increasing amounts of affinity purified WT and DDX5 mutant proteins (Fig. 8C and Supplementary Fig. S9B). The WT and DDX5-D248N proteins exhibited selective and enhanced complex formation with WT but not MT rG4-1 RNA oligonucleotides. By contrast, DDX5-K144N exhibited approximately 10-fold reduced binding to the WT rG4-1 RNA (Fig. 8C), further supporting the requirement of the enzymatic activity of DDX5 in resolving the rG4 structure in the 5'UTR of STAT1 mRNA.

STAT1 expression in liver cancer cell lines and HBV-related liver tumors

To further establish the biological connection between DDX5 and STAT1 protein levels relative to interferon response, we quantified IFN-α response in liver cancer cell lines expressing different levels of DDX5 protein. We compared cell lines Snu387 *vs.* Snu423, and CLC15 *vs*. CLC46 (30), by performing immunoblots of lysates treated with increasing amount of IFN-α for 12h (Fig. 9A

and Fig. S10A). Following quantification of the immunoblots, the signal of DDX5, STAT1, p-STAT1 and IRF9 was normalized to the baseline p-STAT1 signal, obtained without IFN-α treatment (Fig. 9B). The results show the level of STAT1 protein, STAT1 activation, and IFN-α response (IRF9) is proportional to the level of DDX5 (Fig. 9B). Importantly, the basal expression level of STAT1 mRNA is significantly lower in Snu423 cells in comparison to Snu387 cells (Supplementary Fig. S10B).

Next, we analyzed by immunohistochemistry (IHC) the expression of DDX5 and STAT1 proteins in human normal liver tissue, and a small set of HCCs (Fig. 9C) including HBV-related HCCs (Fig. 9D). Normal liver tissue exhibited positive immunostaining for both DDX5 and STAT1, in comparison to other controls. By contrast, HCC1 lacked positive immunostaining for both proteins, whereas HCC2 displayed a weak signal (HCC1 and HCC2 are of unknown etiology). Fig. 9D shows IHC of HBV-related HCCs; we observed absence of immunostaining for both DDX5 and STAT1 in Edmonson's grade 3 HBV-related HCCs, supporting our mechanistic *in vitro* observations.

DDX5 knockdown reduces the antiviral effect of IFN-α on HBV replication

We employed the HBV infection model of dHepaRG cells to examine effect of DDX5 knockdown on HBV replication as a function of IFN-α treatment. dHepaRG cells following establishment of HBV infection, at day 8 p.i., were transfected with siCtrl or siDDX5 , followed by indicated IFN-α starting on day11-17p.i. (Fig. 10A). IFN-α treatment significantly repressed transcription of viral RNAs (Fig. 10B and Supplementary Fig. S11). By contrast, the level of expression of viral RNAs did not become significantly reduced by IFN-α in DDX5 knockdown cells (Fig. 10B and Supplementary Fig. S11). Furthermore, the protein level of STAT1 in response to IFN-α treatment

is reduced in DDX5 knockdown cells in comparison to siCtrl (Fig. 10C). These results support that the protein level or state of activation of DDX5 is a parameter modulating the IFN- α response, in the context of HBV infection.

Discussion

Herein, we report the translational control of STAT1, a transcription factor essential for all types (I/III) of interferon signaling, via a G-quadruplex (rG4) structure located at the 5'UTR of STAT1 mRNA. RNA helicase DDX5 resolves this rG4 structure, thereby enabling STAT1 translation. Significantly, this post-transcriptional regulation of STAT1 expression is a cell intrinsic mechanism that influences the dynamic range of interferon response, dependent on protein level and activity of DDX5. The RNA helicase DDX5 regulates every aspect of RNA metabolism (42), and also serves as a barrier to pluripotency (43). Interestingly, it has been noted that pluripotent stem cells are refractory to interferon signaling (44, 45), although the mechanism is not yet understood. It is currently unknown whether absence of DDX5 expression or activity contributes to lack of innate immune response in pluripotent stem cells (44, 45).

G-quadruplexes (G4) are non-canonical, secondary DNA or RNA structures formed by guanine rich sequences (24, 25, 46). DNA G4 structures are found in gene promoters, particularly of oncogenes, regulating their transcription (47). Interestingly, recent studies demonstrated that DDX5 resolves both RNA and DNA G4 structures, including a G4 structure found in the MYC promoter, enhancing its transcriptional activity (28). RNA G-quadruplexes (rG4) are primarily located in 5'UTR or 3'UTR of mRNAs, playing important roles in RNA biology, from splicing, stability, mRNA targeting, and translation (24, 46). rG4 structures have been identified by various methods in the 5' UTR of NRAS (26), Zic-1(48), Nkx2-5 (49) mRNAs, among other genes (24,

46), regulating their translation. Herein, we demonstrate by pharmacologic, molecular, and biophysical approaches the functional significance of the rG4 structure in the 5'UTR of STAT1 mRNA. Interestingly, this rG4 sequence in the 5'UTR of STAT1 is conserved in primates (Supplementary Fig. S12A), and several polymorphisms are found in the human genome at the 5'UTR of STAT1 (Supplementary Fig. S12B).

We demonstrate that G4-structure stabilizing compounds RR82, PhenDC3 and TMPyP4 reduced the protein level of both STAT1 and NRAS, used as positive control, without affecting STAT1 mRNA level (Fig. 2). After excluding other post-transcriptional modes of STAT1 regulation, we focused on the rG4-1 sequence located in proximity to the 5' end of the STAT1 5'UTR, since it had been identified as a high probability rG4 sequence by the transcriptomic study of Kwok et al (27). Indeed, using an SV40-driven Luciferase reporter, containing the STAT1 5'UTR (nt +1 to +400) upstream from F. Luciferase, we demonstrate that G4-structure stabilizing compounds suppressed the protein synthesis but not mRNA level of the WT rG4-1 containing luciferase vector (Fig. 3). We also edited the genome of Huh7 and HepaRG cells by the CRISPR/Cas9 approach and generated alterations (deletions) of the rG4-1 sequence of STAT1 gene (Fig. 4). When both alleles harbored the edited rG4-1 sequence, as in HepaRG clone C5, STAT1 protein levels were increased. Significantly, expression of STAT1 in clone C5 was resistant both to DDX5 knockdown (Fig. 5A), and the inhibitory effect of G4-stabilizing compounds (Fig. 5B). Circular dichroism and thermal stability measurements directly demonstrated formation of G-quadruplex only by WT and C9 rG4-1 sequences (Fig. 6), supporting the biological data. RIP assays using antibody to endogenous DDX5 protein, showed lack of DDX5 binding to STAT1 mRNA from clone C5, containing edited rG4-1 sequence in both alleles. By contrast, DDX5 bound to STAT1 mRNA encoding the WT and C9 rG4-1 sequence (Fig. 7).

Importantly, the RNA helicase activity of DDX5 is required for binding STAT1 mRNA, shown by the reduced STAT1 mRNA binding of the DDX5-K144N mutant that lacks ATPase activity (Fig. 7). These results were further verified by RNA pulldown assays using synthetic RNA oligonucleotides under K+ conditions enabling formation of the G-quadruplex structure, thereby confirming endogenous DDX5 recognizes the G-quadruplex found at the 5' UTR of STAT1 mRNA (Fig. 8). Moreover, employing pull-down assays we further confirmed the enzymatic activity of DDX5, modeled by DDX5- K144N mutant, is required for WT rG4-1 binding (Fig. 8). In addition, EMSAs directly demonstrated complex formation between the WT rG4-1 RNA and DDX5, while DDX5-K144N exhibited significantly reduced complex formation. (Fig. 8).Taken these results together, we conclude, the rG4-1 sequence in 5'UTR of human STAT1 mRNA assumes a G-quadruplex secondary structure. This rG4 structure, stabilized by G4-stabilizing compounds RR82, PhenDC3 and TMPyP4, suppresses STAT1 mRNA translation. RNA helicase DDX5 resolves the rG4 structure, enabling STAT1 mRNA translation.

Regarding the biological significance of this mechanism, first, we compared STAT1 levels and the interferon response using two sets of liver cancer cell lines expressing low *vs.* high DDX5, namely, Snu387 *vs.* Snu423, and CCL15 and CCL46 derived from HBV-related HCCs (30). We observed, the magnitude of the IFN-α response is a cell intrinsic property, dependent on DDX5 (Fig. 9A-B and Fig. S10). Although the ATPase activity of DDX5 (42) is required for binding to STAT1 mRNA (Fig. 8), recent studies have shown that PRMT5-mediated arginine methylation of DDX5 modulates its function in resolving DNA:RNA hybrids (50). However, how the activity of DDX5 is regulated in different cellular contexts or in response to interferon, is presently not understood (Fig. S13). Certainly, the regulation of DDX5 will add another level of complexity to this novel mechanism of interferon response. In the context of HBV infection and interferon

treatment, knockdown of DDX5 reduced the antiviral effect of IFN-α, via STAT1 protein reduction (Fig. 10). However, a lot remains to be understood of STAT1 regulation. Specifically, recent studies have identified additional mechanisms that regulate STAT1 mRNA stability and translation, involving lncRNA Sros1 and RNA binding protein CAPRIN1, in response to IFN-γ (51).Thus, STAT1 expression involves multipronged regulation, the integration of which remains to be understood.

We also show that in comparison to normal liver, in HCCs and HBV-related HCCs analyzed herein, the absence of DDX5 also corresponds to absence of STAT1 immunostaining (Fig. 9). Absence of STAT1 expression could provide an explanation for the lack of IFN-α response observed in many chronically HBV infected patients with HCC (16). Interestingly, a positive indicator for IFN-α responsiveness in HBV-infected patients with HCC (16) is expression of IFIT3, a STAT1 regulated gene (15). In addition, it is presently unknown whether this mechanism of DDX5-dependent STAT1 translational regulation is also linked to the immunotherapy response of patients with HCCs. Our earlier studies identified downregulation of DDX5 to be associated with poor prognosis HBV-related HCC (18), and hepatocyte reprogramming to a less-differentiated state exhibiting features of hCSCs (23), in agreement with the role of DDX5 as a barrier to pluripotency (43). Regarding immunotherapy which is based on PD-1 blockade, the PD-L1,2 ligands are induced in tumors by interferon gamma, leading to immune evasion (52). According to the mechanism described herein, absence or downregulation of DDX5 in HCCs will result in absence or reduced protein of STAT1, and in turn reduced PD-L1 expression (52).

References

1. Stark GR, Darnell JE, Jr. The JAK-STAT pathway at twenty. Immunity 2012;36:503-514.
2. Stanifer ML, Pervolaraki K, Boulant S. Differential Regulation of Type I and Type III Interferon Signaling. Int J Mol Sci 2019;20.
3. Chen K, Liu J, Liu S, Xia M, Zhang X, Han D, Jiang Y, et al. Methyltransferase SETD2-Mediated Methylation of STAT1 Is Critical for Interferon Antiviral Activity. Cell 2017;170:492-506 e414.
4. Kramer OH, Knauer SK, Greiner G, Jandt E, Reichardt S, Guhrs KH, Stauber RH, et al. A phosphorylation-acetylation switch regulates STAT1 signaling. Genes Dev 2009;23:223-235.
5. Liu S, Jiang M, Wang W, Liu W, Song X, Ma Z, Zhang S, et al. Nuclear RNF2 inhibits interferon function by promoting K33-linked STAT1 disassociation from DNA. Nat Immunol 2018;19:41-52.
6. Schneider WM, Chevillotte MD, Rice CM. Interferon-stimulated genes: a complex web of host defenses. Annu Rev Immunol 2014;32:513-545.
7. Ladner SK, Otto MJ, Barker CS, Zaifert K, Wang GH, Guo JT, Seeger C, et al. Inducible expression of human hepatitis B virus (HBV) in stably transfected hepatoblastoma cells: a novel system for screening potential inhibitors of HBV replication. Antimicrob Agents Chemother 1997;41:1715-1720.
8. Lucifora J, Durantel D, Testoni B, Hantz O, Levrero M, Zoulim F. Control of hepatitis B virus replication by innate response of HepaRG cells. Hepatology 2010;51:63-72.
9. Bruix J, Qin S, Merle P, Granito A, Huang YH, Bodoky G, Pracht M, et al. Regorafenib for patients with hepatocellular carcinoma who progressed on sorafenib treatment (RESORCE): a randomised, double-blind, placebo-controlled, phase 3 trial. Lancet 2017;389:56-66.
10. Abou-Alfa GK, Meyer T, Cheng AL, El-Khoueiry AB, Rimassa L, Ryoo BY, Cicin I, et al. Cabozantinib in Patients with Advanced and Progressing Hepatocellular Carcinoma. N Engl J Med 2018;379:54-63.
11. Llovet JM, Bruix J. Molecular targeted therapies in hepatocellular carcinoma. Hepatology 2008;48:1312-1327.
12. Taniguchi T, Takaoka A. A weak signal for strong responses: interferon-alpha/beta revisited. Nat Rev Mol Cell Biol 2001;2:378-386.
13. Platanias LC. Mechanisms of type-I- and type-II-interferon-mediated signalling. Nat Rev Immunol 2005;5:375-386.
14. Lebosse F, Testoni B, Fresquet J, Facchetti F, Galmozzi E, Fournier M, Hervieu V, et al. Intrahepatic innate immune response pathways are downregulated in untreated chronic hepatitis B. J Hepatol 2017;66:897-909.
15. Xiao S, Li D, Zhu HQ, Song MG, Pan XR, Jia PM, Peng LL, et al. RIG-G as a key mediator of the antiproliferative activity of interferon-related pathways through enhancing p21 and p27 proteins. Proc Natl Acad Sci U S A 2006;103:16448-16453.
16. Yang Y, Zhou Y, Hou J, Bai C, Li Z, Fan J, Ng IOL, et al. Hepatic IFIT3 predicts interferon-alpha therapeutic response in patients of hepatocellular carcinoma. Hepatology 2017;66:152-166.
17. Zhang H, Diab A, Fan H, Mani SK, Hullinger R, Merle P, Andrisani O. PLK1 and HOTAIR Accelerate Proteasomal Degradation of SUZ12 and ZNF198 during Hepatitis B Virus-Induced Liver Carcinogenesis. Cancer Res 2015;75:2363-2374.
18. Zhang H, Xing Z, Mani SK, Bancel B, Durantel D, Zoulim F, Tran EJ, et al. RNA helicase DEAD box protein 5 regulates Polycomb repressive complex 2/Hox transcript antisense intergenic RNA function in hepatitis B virus infection and hepatocarcinogenesis. Hepatology 2016;64:1033-1048.
19. Mani SKK, Andrisani O. Hepatitis B Virus-Associated Hepatocellular Carcinoma and Hepatic Cancer Stem Cells. Genes (Basel) 2018;9.
20. Margueron R, Reinberg D. The Polycomb complex PRC2 and its mark in life. Nature 2011;469:343-349.

21. Jarmoskaite I, Russell R. RNA helicase proteins as chaperones and remodelers. Annu Rev Biochem 2014;83:697-725.
22. Jankowsky E, Fairman ME. RNA helicases--one fold for many functions. Curr Opin Struct Biol 2007;17:316-324.
23. Mani SKK, Yan B, Cui Z, Sun J, Utturkar S, Foca A, Fares N, et al. Restoration of RNA helicase DDX5 suppresses hepatitis B virus (HBV) biosynthesis and Wnt signaling in HBV-related hepatocellular carcinoma. Theranostics 2020;10:10957-10972.
24. Bugaut A, Balasubramanian S. 5'-UTR RNA G-quadruplexes: translation regulation and targeting. Nucleic Acids Res 2012;40:4727-4741.
25. Yang D. G-Quadruplex DNA and RNA. Methods Mol Biol 2019;2035:1-24.
26. Kumari S, Bugaut A, Huppert JL, Balasubramanian S. An RNA G-quadruplex in the 5' UTR of the NRAS proto-oncogene modulates translation. Nat Chem Biol 2007;3:218-221.
27. Kwok CK, Marsico G, Sahakyan AB, Chambers VS, Balasubramanian S. rG4-seq reveals widespread formation of G-quadruplex structures in the human transcriptome. Nat Methods 2016;13:841-844.
28. Wu G, Xing Z, Tran EJ, Yang D. DDX5 helicase resolves G-quadruplex and is involved in MYC gene transcriptional activation. Proc Natl Acad Sci U S A 2019;116:20453-20461.
29. Lucifora J, Durantel D, Belloni L, Barraud L, Villet S, Vincent IE, Margeridon-Thermet S, et al. Initiation of hepatitis B virus genome replication and production of infectious virus following delivery in HepG2 cells by novel recombinant baculovirus vector. J Gen Virol 2008;89:1819-1828.
30. Qiu Z, Li H, Zhang Z, Zhu Z, He S, Wang X, Wang P, et al. A Pharmacogenomic Landscape in Human Liver Cancers. Cancer Cell 2019;36:179-193 e111.
31. Gripon P, Rumin S, Urban S, Le Seyec J, Glaise D, Cannie I, Guyomard C, et al. Infection of a human hepatoma cell line by hepatitis B virus. Proc Natl Acad Sci U S A 2002;99:15655-15660.
32. Hatzakis E, Okamoto K, Yang D. Thermodynamic stability and folding kinetics of the major G-quadruplex and its loop isomers formed in the nuclease hypersensitive element in the human c-Myc promoter: effect of loops and flanking segments on the stability of parallel-stranded intramolecular G-quadruplexes. Biochemistry 2010;49:9152-9160.
33. Yang L, Yang JL, Byrne S, Pan J, Church GM. CRISPR/Cas9-Directed Genome Editing of Cultured Cells. Curr Protoc Mol Biol 2014;107:31 31 31-17.
34. Zhu X, Xu Y, Yu S, Lu L, Ding M, Cheng J, Song G, et al. An efficient genotyping method for genome-modified animals and human cells generated with CRISPR/Cas9 system. Sci Rep 2014;4:6420.
35. Ribeiro de Almeida C, Dhir S, Dhir A, Moghaddam AE, Sattentau Q, Meinhart A, Proudfoot NJ. RNA Helicase DDX1 Converts RNA G-Quadruplex Structures into R-Loops to Promote IgH Class Switch Recombination. Mol Cell 2018;70:650-662 e658.
36. Han FX, Wheelhouse RT, Hurley LH. Interactions of TMPyP4 and TMPyP2 with Quadruplex DNA. Structural Basis for the Differential Effects on Telomerase Inhibition. Journal of the American Chemical Society 1999;121:3561-3570.
37. Kumari S, Bugaut A, Balasubramanian S. Position and stability are determining factors for translation repression by an RNA G-quadruplex-forming sequence within the 5' UTR of the NRAS proto-oncogene. Biochemistry 2008;47:12664-12669.
38. Lander ES. The Heroes of CRISPR. Cell 2016;164:18-28.
39. Del Villar-Guerra R, Gray RD, Chaires JB. Characterization of Quadruplex DNA Structure by Circular Dichroism. Curr Protoc Nucleic Acid Chem 2017;68:17 18 11-17 18 16.
40. Zhang J, Lau MW, Ferré-D'Amaré AR. Ribozymes and Riboswitches: Modulation of RNA Function by Small Molecules. Biochemistry 2010;49:9123-9131.
41. Jalal C, Uhlmann-Schiffler H, Stahl H. Redundant role of DEAD box proteins p68 (Ddx5) and p72/p82 (Ddx17) in ribosome biogenesis and cell proliferation. Nucleic Acids Res 2007;35:3590-3601.

42. Linder P, Jankowsky E. From unwinding to clamping - the DEAD box RNA helicase family. Nat Rev Mol Cell Biol 2011;12:505-516.
43. Li H, Lai P, Jia J, Song Y, Xia Q, Huang K, He N, et al. RNA Helicase DDX5 Inhibits Reprogramming to Pluripotency by miRNA-Based Repression of RYBP and its PRC1-Dependent and -Independent Functions. Cell Stem Cell 2017;20:571.
44. Guo L, Lin L, Wang X, Gao M, Cao S, Mai Y, Wu F, et al. Resolving Cell Fate Decisions during Somatic Cell Reprogramming by Single-Cell RNA-Seq. Mol Cell 2019;73:815-829 e817.
45. Guo YL, Carmichael GG, Wang R, Hong X, Acharya D, Huang F, Bai F. Attenuated Innate Immunity in Embryonic Stem Cells and Its Implications in Developmental Biology and Regenerative Medicine. Stem Cells 2015;33:3165-3173.
46. Millevoi S, Moine H, Vagner S. G-quadruplexes in RNA biology. Wiley Interdiscip Rev RNA 2012;3:495-507.
47. Qin Y, Hurley LH. Structures, folding patterns, and functions of intramolecular DNA G-quadruplexes found in eukaryotic promoter regions. Biochimie 2008;90:1149-1171.
48. Arora A, Dutkiewicz M, Scaria V, Hariharan M, Maiti S, Kurreck J. Inhibition of translation in living eukaryotic cells by an RNA G-quadruplex motif. RNA 2008;14:1290-1296.
49. Nie J, Jiang M, Zhang X, Tang H, Jin H, Huang X, Yuan B, et al. Post-transcriptional Regulation of Nkx2-5 by RHAU in Heart Development. Cell Rep 2015;13:723-732.
50. Mersaoui SY, Yu Z, Coulombe Y, Karam M, Busatto FF, Masson JY, Richard S. Arginine methylation of the DDX5 helicase RGG/RG motif by PRMT5 regulates resolution of RNA:DNA hybrids. Embo j 2019;38:e100986.
51. Xu H, Jiang Y, Xu X, Su X, Liu Y, Ma Y, Zhao Y, et al. Inducible degradation of lncRNA Sros1 promotes IFN-γ-mediated activation of innate immune responses by stabilizing Stat1 mRNA. Nat Immunol 2019;20:1621-1630.
52. Garcia-Diaz A, Shin DS, Moreno BH, Saco J, Escuin-Ordinas H, Rodriguez GA, Zaretsky JM, et al. Interferon Receptor Signaling Pathways Regulating PD-L1 and PD-L2 Expression. Cell Rep 2017;19:1189-1201.
53. Diab A, Foca A, Fusil F, Lahlali T, Jalaguier P, Amirache F, N'Guyen L, et al. Polo-like-kinase 1 is a proviral host factor for hepatitis B virus replication. Hepatology 2017;66:1750-1765.

Figure legends

Figure 1. DDX5 knockdown regulates STAT1 mRNA translation. (A) Immunoblots of IFN-α induced proteins using lysates from HepAD38 cells with (+) or without (-) HBV replication for 5 days as a function of IFN-α (500 ng/ml) treatment for the last 24 h. (Right panel) quantification of DDX5 and STAT1 protein level, by ImageJ software, from three independent biological replicates. *: $p<0.05$, **: $p<0.01$; Error bars indicate Mean ±SEM. Immunoblot of indicated proteins in: **(B)** HepAD38, Huh7 and HepaRG cells transfected with DDX5 siRNAs (siDDX5-1 or siDDX5-2) or negative control siRNA (siCtrl) for 48 h, and **(C)** in WT and DDX5 knockdown ($DDX5^{KD}$) HepAD38 cell lines KD2, KD3 and KD5. **(D)-(F)** qRT-PCR of HBV pgRNA and STAT1 mRNA, as indicated, using RNA from: **(D)** HepAD38 cells with (+) or without (-) HBV replication for 5 days; **(E)** WT and KD5 HepAD38 cells (left panel), and WT and KD5 HepAD38 cells transfected with siSTAT1 or siCtrl for 48 h (right panel); and **(F)** HepAD38, Huh7, and HepaRG cells transfected with siDDX5 or siCtrl for 48h. Statistical analysis of DDX5 and STAT1 mRNA levels from three biological replicates. *: $p<0.05$, ns: not significant; Error bars indicate Mean ±SEM.

Figure 2. G-quadruplex stabilizing drugs reduce STAT1 protein levels. (A) Chemical structure of G4 stabilizing compounds PhenDC3, RR82, TMPyP4 and TMPyP2. **(B)** Immunoblots of STAT1, NRAS and DDX5, using lysates from HepAD38 cells treated for 48 h with PhenDC3 (5 μM) or RR82 (5 μM). (Lower panel) qRT-PCR of STAT1 mRNA using RNA from HepAD38 cells treated with DMSO, PhenDC3 (5 μM) or RR82 (5 μM) for 48 h. **(C)** Immunoblots of STAT1 from lysates of HepAD38 and Huh7 cells treated with TMPyP4 (5 μM) or TMPyP2 (5 μM) for 48h. (Lower panel), qRT-PCR of STAT1 mRNA from HepAD38 and Huh7 cells, treated as

indicated. Statistical analysis of STAT1 mRNA is from three biological replicates. ns: not significant; Error bars indicate Mean ±SEM.

Figure 3. G-quadruplex (rG4) regulates STAT1 expression post-transcriptionally. (A) Human STAT1 5'UTR upstream of Firefly (F.) Luciferase reporter, driven from SV40 promoter. Putative rG4 sequences in 5' UTR indicated as rG4-1, rG4-2 and rG4-3. WT rG4-1 nucleotide sequence is shown. Italics indicate site-directed changes in mutant MT-rG4-1. **(B)** - **(E)** Ratio of Firefly/Renilla luciferase activity at 24 h after co-transfection of WT or MT STAT1-5'UTR-F. Luciferase and Renilla-Luciferase expression plasmids. Lower panels, ratio of Firefly/Renilla luciferase mRNAs quantified by qRT-PCR. **(B)** HepAD38 and Huh7 cells. **(C)** HepAD38 cells with (+) or without (-) HBV replication for 5 days. **(D)** HepAD38 cells, and **(E)** Huh7 cells treated with indicated G-quadruplex stabilizing drugs (5 μM) for 24 h. Statistical analysis from three independent biological replicates. *: $p<0.05$, **: $p<0.01$, ***: $p<0.001$, ns: not significant; Error bars indicate Mean ±SEM.

Figure 4. Genomic editing of rG4-1 increases STAT1 protein levels. (A) Sequence of CRIPSR/Cas9 edited rG4-1 sequence in **(A)** Huh7 and **(B)** HepaRG cells. Immunoblot of STAT1 in indicated cell lines. Right panels, quantification of STAT1 protein by ImageJ software, and qRT-PCR of STAT1 mRNA, from three independent biological replicates. *: $p<0.05$, ns: not significant; Error bars indicate Mean ±SEM.

Figure 5. Effect of G-quadruplex stabilizing drugs on rG4-1 edited HepaRG cells. Immunoblots of indicated proteins using lysates from indicated HepaRG cells (WT, C5, and C9). **(A)** After transfection of siCtrl or siDDX5 RNA for 48 h; **(B)** following treatment with RR82 (5 μM), TMPyP4 (5 μM) or TMPyP2 (5 μM) for 48 h, and **(C)** treatment with RR82 (5 μM) for 48 h

in combination with IFN-α (500 ng/ml) for the last 24 h. Quantification (**A-C)** from three independent biological replicates. *: $p<0.05$, **: $p<0.01$, ***: $p<0.001$, ns: not significant. Error bars indicate Mean ±SEM.

Figure 6. The rG4-1 sequence in 5'UTR of STAT1 mRNA forms G-quadruplex. (A) Synthetic RNA oligonucleotides of WT STAT1 rG4-1 and corresponding mutants in HepaRG clones C5 and C9. **(B)** CD spectroscopy measurement, and **(C)** melting curves of RNA oligonucleotides annealed by heating to 95ºC and slowly cooled down to room temperature. (**D)** Melting temperature (Tm), without and with (100 mM) KCl, calculated from **A-C.**

Figure 7. DDX5 binds STAT1 mRNA. Ribonucleoprotein immunoprecipitation (RIP) assays with DDX5 antibody performed in **(A)** HepAD38, Huh7, and **(B)** HepaRG WT, C5 and C9 cells. DDX5 enriched RNAs quantified by qRT-PCR using STAT1 primers. Results are from three biological replicates. *: $p<0.05$, ns=not significant. **(C)** RIP assays with FLAG antibody performed using HepaRG-DDX5-WT-FLAG, HepaRG-DDX5-K144N-FLAG and HepaRG-DDX5-D248N-FLAG expressing cell lines. FLAG antibody immunoprecipitated RNAs quantified by qRT-PCR using STAT1 primers. Results are from three biological replicates. *: $p<0.05$, ns=not significant.

Figure 8. DDX5 binds rG4-1 structure of 5'UTR of STAT1 mRNA (A) (Upper panel) Sequence of synthetic biotinylated RNA oligonucleotides, Bio-rG4 and Bio-rG4mut. (Lower panel) RNA pulldown assays using Bio-rG4 and Bio-rG4mut in 100 mM KCl or 100 mM LiCl, bound to lysates from indicated cell lines, followed by immunoblots with DDX5 antibody. **(B)** RNA pulldown assays using Bio-rG4 and Bio-rG4mut in 100 mM KCl, bound to lysates from HepaRG-DDX5-WT-FLAG, HepaRG-DDX5-K144N-FLAG and HepaRG-DDX5-D248N-FLAG expressing cell lines, followed by immunoblots with FLAG antibody. A representative assay is shown from three independent experiments. Band intensities quantified by ImageJ. Results are from three biological

replicates. **: p<0.01, ns=not significant. **(C)** EMSA using Bio-rG4 and Bio-rG4mut RNA oligonucleotides, in binding reactions containing indicated amount of immunoaffinity purified DDX5-WT, DDX5-K144N, and DDX5-D248N, analyzed by native gel electrophoresis in 1.5% agarose gels, and visualized by staining with SYBR™-Gold dye (ThermoFisher) and ChemiDoc™ Touch Imaging System.

Figure 9. DDX5 expression level in liver cancer cell lines and liver tumors. (A) Immunoblots using lysates from indicated cell lines treated with IFN-α (100 and 500 ng/ml) for 12 h. **(B)** Quantification shows ratio of DDX5, STAT1, p-STAT1, and IRF9 and relative to level of p-STAT1 in IFN-α untreated cells. Results are average from three independent experiments. (**C)** Immunohistrochemistry of normal liver, HCCs, and **(D)** HBV-related HCCs, performed as described (18). NSCLC (Non-small cell lung cancer) tissue and normal human colon tissue were used as positive controls, as indicated, with DDX5 and STAT1 antibodies *vs.* IgG.

Figure 10. DDX5 knockdown reduces antiviral IFN-α effect on HBV replication. (A) Diagram illustrates the workflow of HBV infection using dHepaRG cells; infection with HBV was carried out at moi=500 in the presence of 4% Peg8000, in triplicates. siRNAs (25 nM) control (siCtrl) or DDX5 (Dharmacon) transfected on day8 p.i. IFN-α added on days 11 and 14 p.i.**(B)** Quantification of total HBV RNA and pgRNA by qRT-PCR as previously described (53). Results are from two independent experiments performed in triplicates. *p<0.05 **(C)** Immunoblots of WCE from HBV infected cells, with indicated antibodies. Relative Intensity (Rel. int.) is the ratio of STAT1/actin, quantified by image J software. A representative assay is shown from two independent experiments.

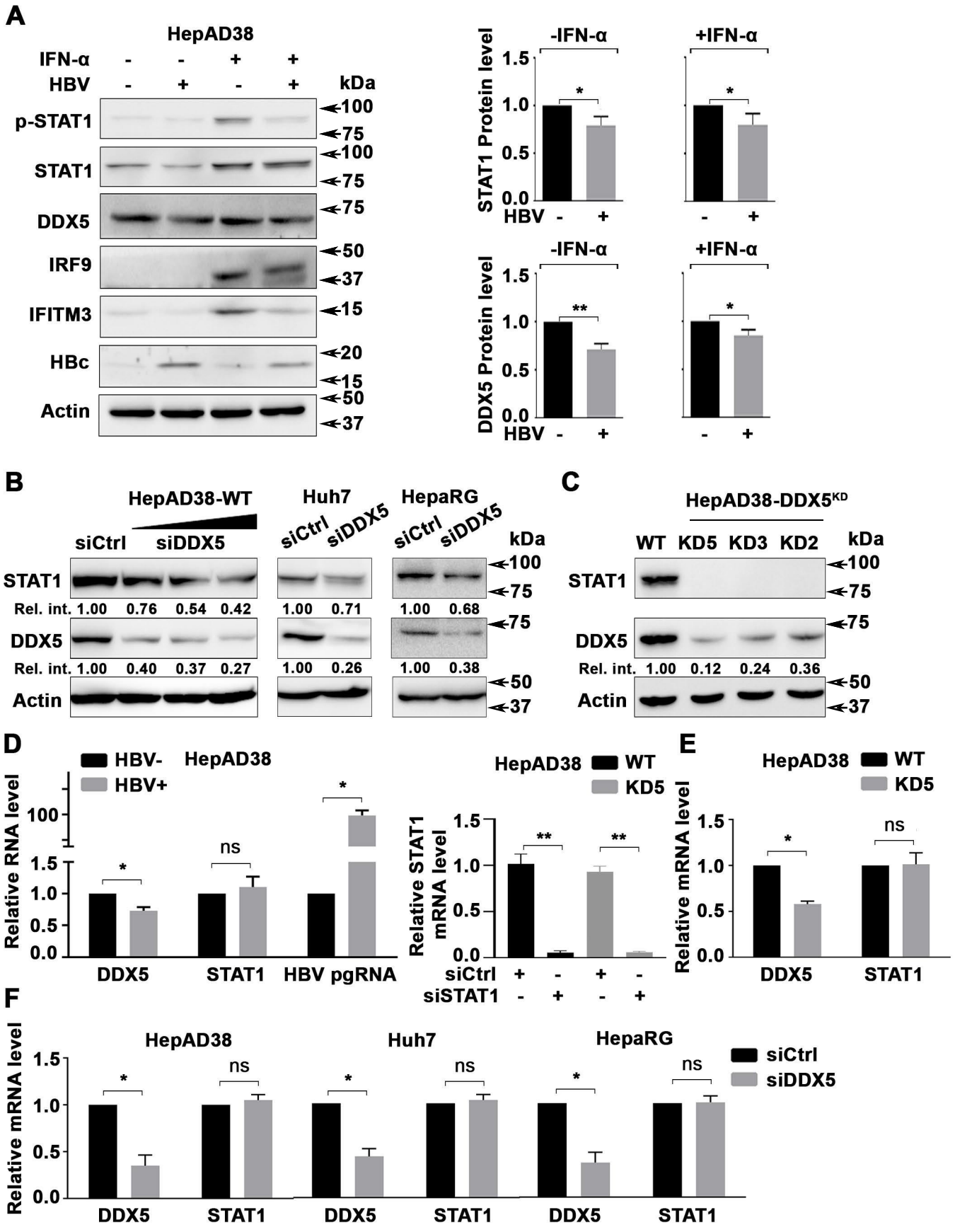
A
HepAD38
IFN-α - - + +
HBV - + - +
kDa
p-STAT1
STAT1
DDX5
IRF9
IFITM3
HBc
Actin
100
75
50
37
15
20
-IFN-α
+IFN-α
STAT1 Protein level
DDX5 Protein level
B
HepAD38-WT
siCtrl
siDDX5
Huh7
HepaRG
Rel. int. 1.00 0.76 0.54 0.42
1.00 0.71
1.00 0.68
Rel. int. 1.00 0.40 0.37 0.27
1.00 0.26
1.00 0.38
C
HepAD38-DDX5KD
WT KD5 KD3 KD2
Rel. int. 1.00 0.12 0.24 0.36
D
HBV- HepAD38
HBV+
Relative RNA level
DDX5
STAT1
HBV pgRNA
HepAD38 WT KD5
Relative STAT1 mRNA level
siCtrl
siSTAT1
E
HepAD38 WT KD5
Relative mRNA level
F
HepAD38
Huh7
HepaRG
siCtrl
siDDX5

Figure 1

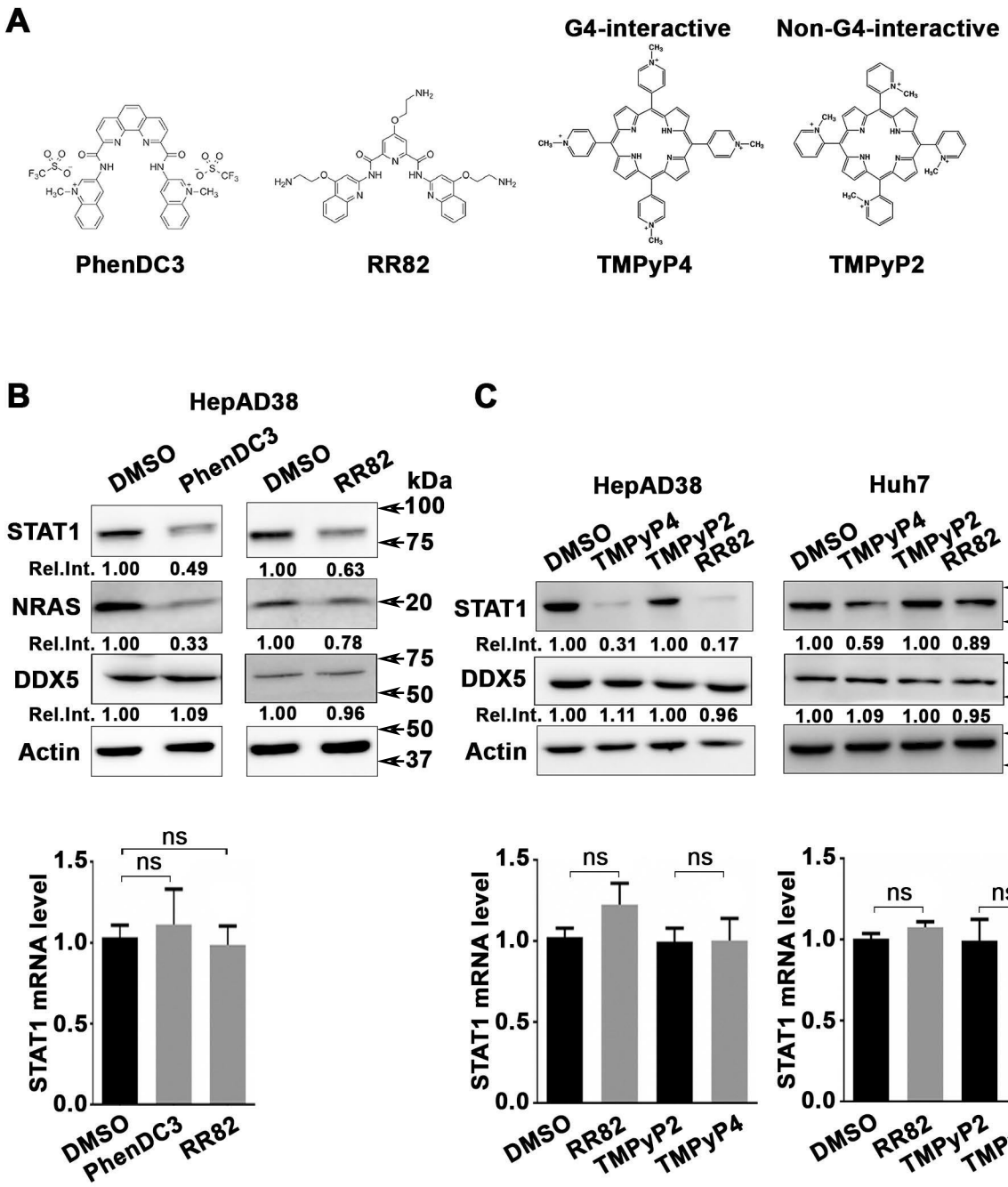
A
G4-interactive
Non-G4-interactive
PhenDC3
RR82
TMPyP4
TMPyP2
B
HepAD38
DMSO
PhenDC3
DMSO
RR82
kDa
STAT1
Rel.Int. 1.00 0.49 1.00 0.63
NRAS
Rel.Int. 1.00 0.33 1.00 0.78
DDX5
Rel.Int. 1.00 1.09 1.00 0.96
Actin
100
75
20
75
50
50
37
ns
ns
STAT1 mRNA level
1.5
1.0
0.5
0.0
DMSO
PhenDC3
RR82
C
HepAD38
Huh7
DMSO
TMPyP4
TMPyP2
RR82
kDa
STAT1
Rel.Int. 1.00 0.31 1.00 0.17
1.00 0.59 1.00 0.89
DDX5
Rel.Int. 1.00 1.11 1.00 0.96
1.00 1.09 1.00 0.95
Actin
100
75
75
50
50
37
ns
STAT1 mRNA level
DMSO
RR82
TMPyP2
TMPyP4

Figure 2

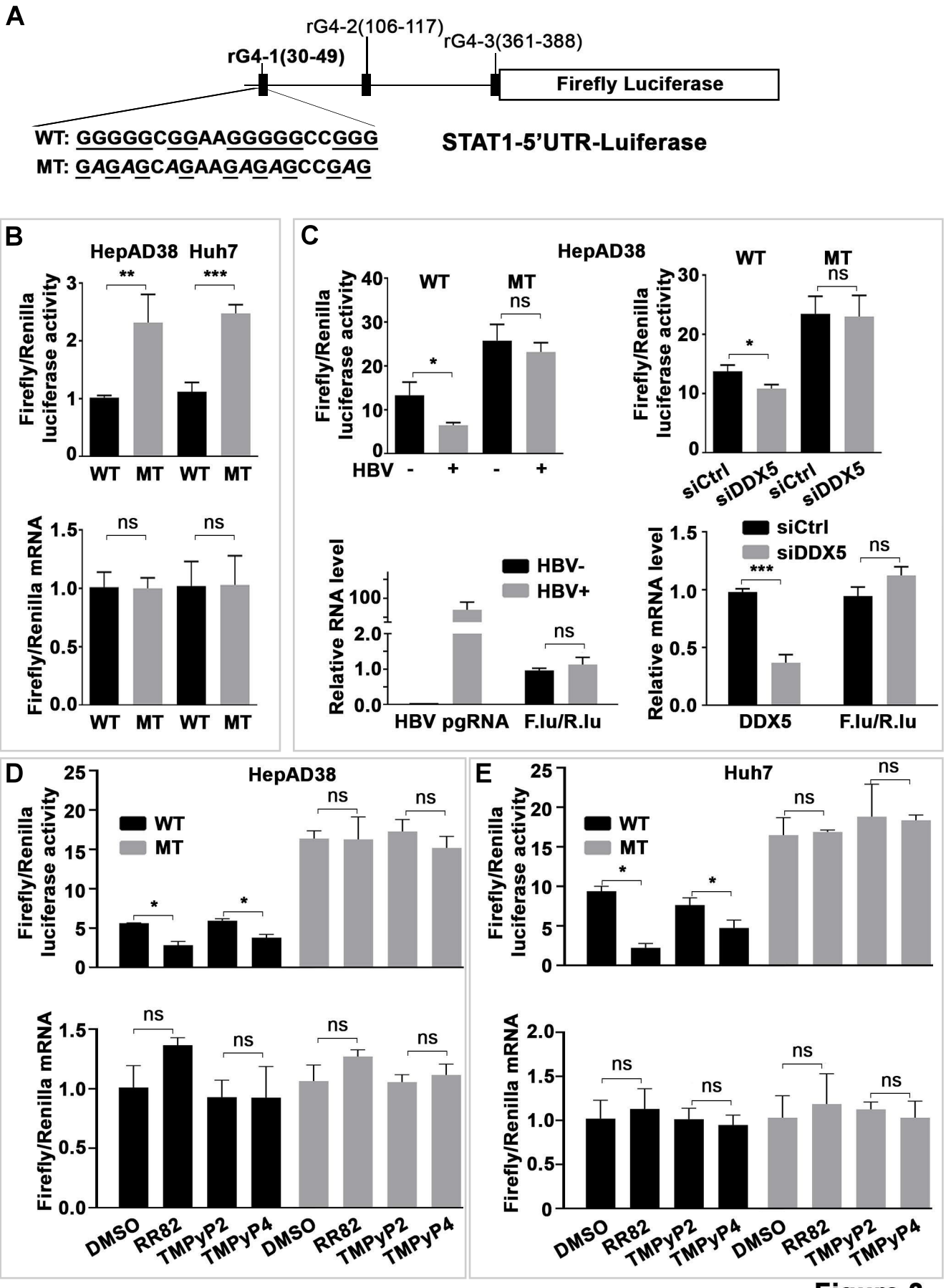
A
rG4-2(106-117)
rG4-1(30-49)
rG4-3(361-388)
Firefly Luciferase
WT: GGGGGCGGAAGGGGGCCGGG
MT: GAGAGCAGAAGAGAGCCGAG
STAT1-5'UTR-Luiferase
B
HepAD38 Huh7
Firefly/Renilla luciferase activity
Firefly/Renilla mRNA
WT MT WT MT
ns
C
HepAD38
WT MT
HBV - + - +
siCtrl siDDX5 siCtrl siDDX5
Relative RNA level
HBV pgRNA F.lu/R.lu
HBV-
HBV+
siCtrl
siDDX5
Relative mRNA level
DDX5 F.lu/R.lu
D
HepAD38
WT
MT
DMSO RR82 TMPyP2 TMPyP4 DMSO RR82 TMPyP2 TMPyP4
E
Huh7

Figure 3

A

Huh7 CRISPR edited clones

WT rG4-1: 5'…CCCGGTGATTGGTGGGGGCGGAAGGGGGCCGGG…3'
17 nt 49 nt

C17 rG4-1, allele 1: 5'…CCCGGTGATT……..…GGCGG……GGGCCGGG…3'

C17 rG4-1, allele 2: 5'…CCCGGTGATT…....GGGGGCGGAAGGGGGCCGGG…3'

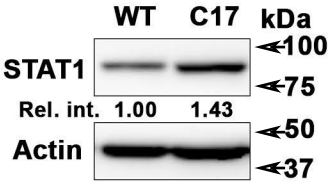

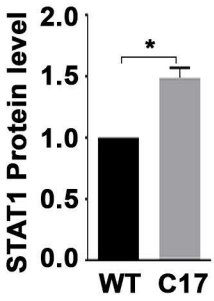

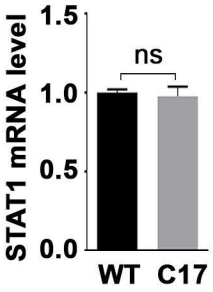

B

HepaRG CRISPR edited clones

WT rG4-1: 5'…CCCGGTGATTGGTGGGGGCGGAAGGGGGCCGGG…3'
17 nt 49 nt

C5 rG4-1, allele 1: 5'…CCC.……CGGAAGGGGGCCGGG…3'

C5 rG4-1, allele 2: 5'…CCC.…….....GGGGCCGGG…3'

C9 rG4-1, allele 1: 5'…CCCGGTGATT.....GGGGGCGGAAGGGGGCCGGG…3'

C9 rG4-1, allele 2: 5'…CCCGGTGATTGGT.....GGGGGCCGGG…3'

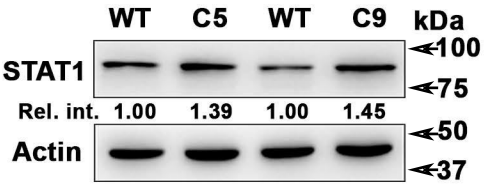

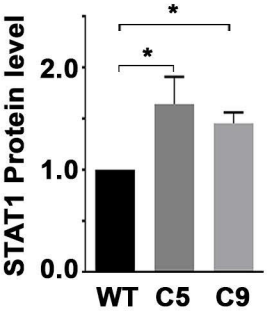

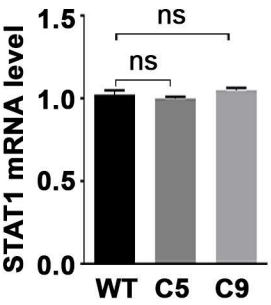

Figure 4

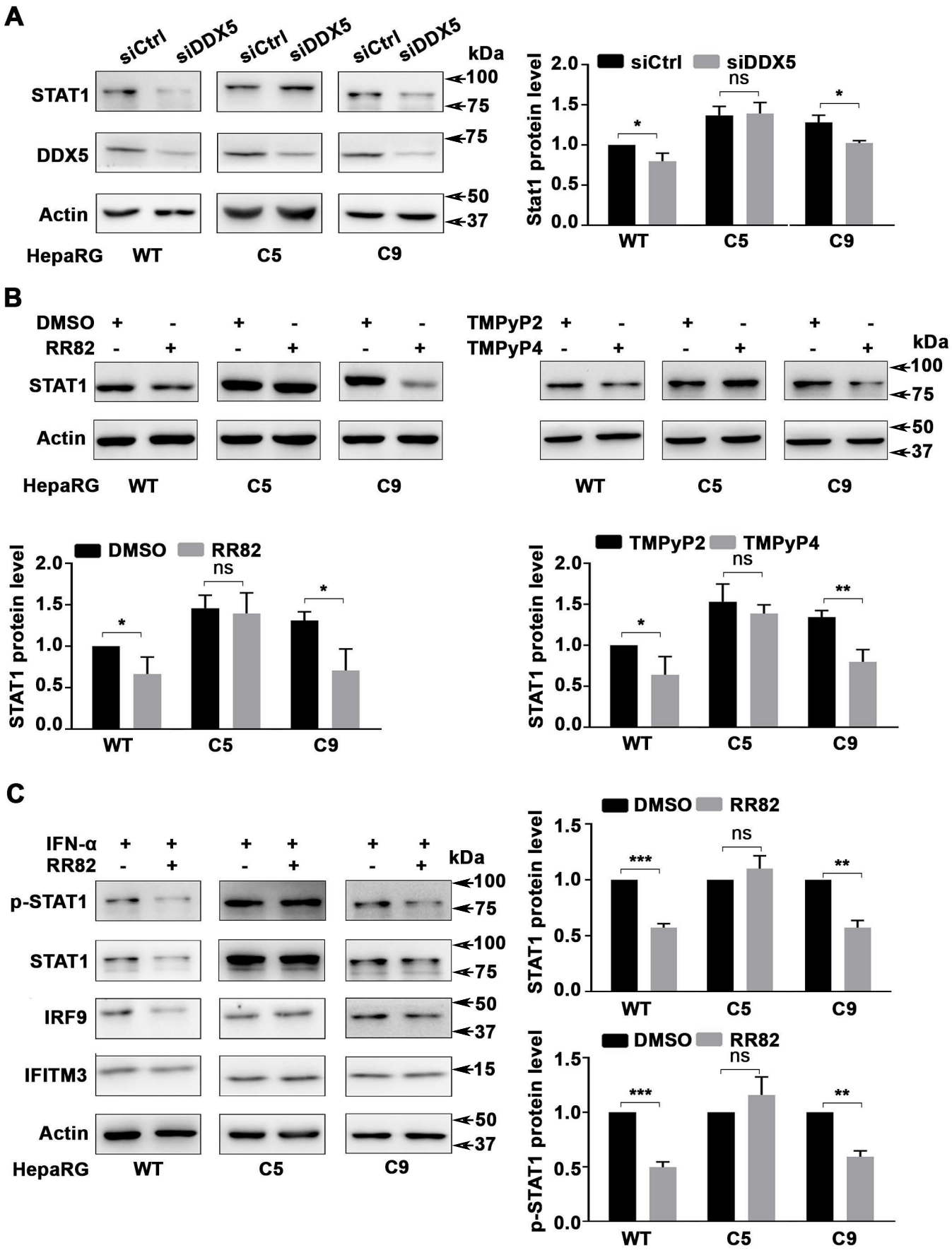
A
siCtrl
siDDX5
siCtrl
siDDX5
siCtrl
siDDX5
kDa
STAT1
DDX5
Actin
100
75
75
50
37
HepaRG
WT
C5
C9
Stat1 protein level
siCtrl
siDDX5
ns
B
DMSO
RR82
TMPyP2
TMPyP4
STAT1
Actin
STAT1 protein level
DMSO
RR82
TMPyP2
TMPyP4
C
IFN-α
RR82
p-STAT1
STAT1
IRF9
IFITM3
Actin
15
p-STAT1 protein level

Figure 5

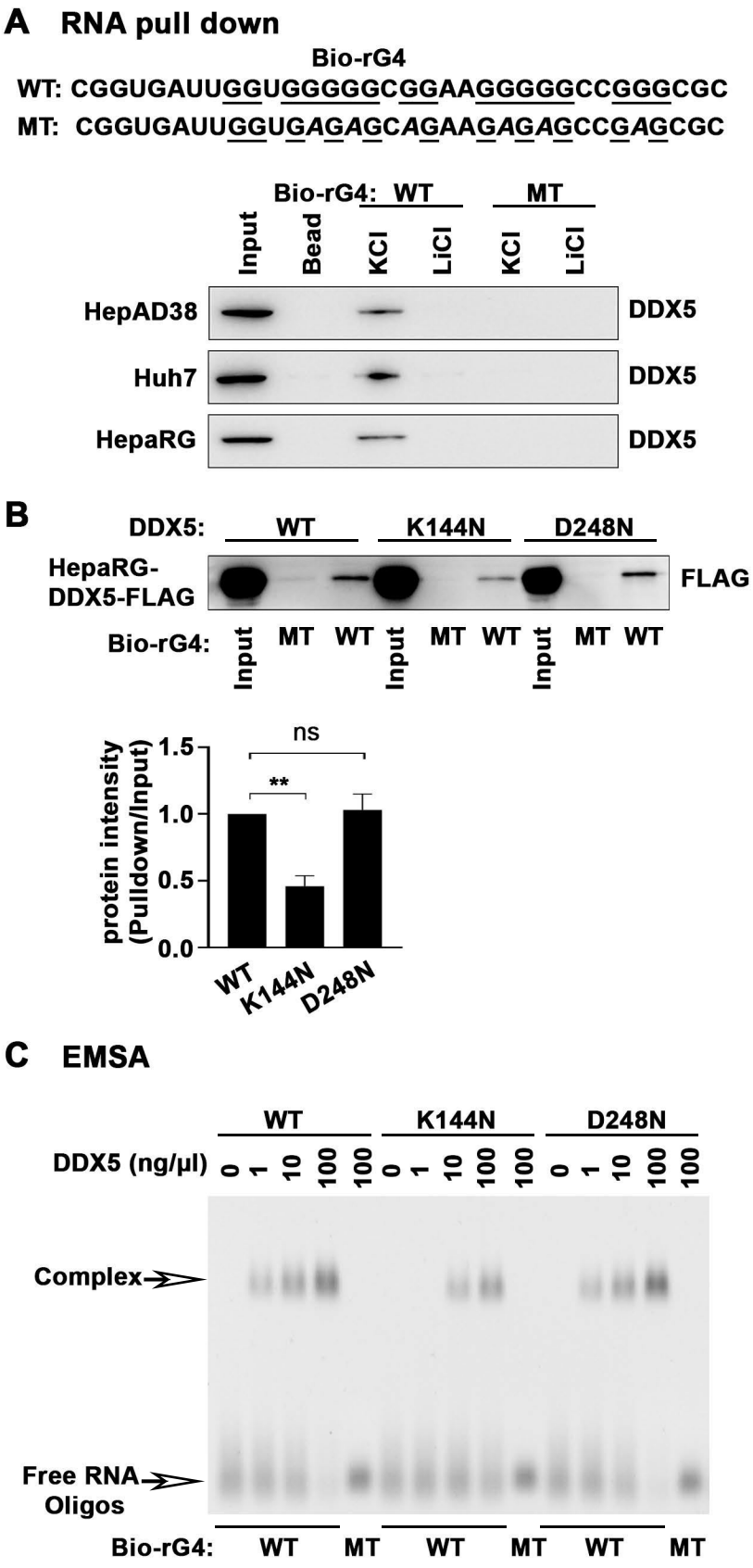
A RNA pull down
Bio-rG4
WT: CGGUGAUUGGUGGGGGCGGAAGGGGGCCGGGCGC
MT: CGGUGAUUGGUGAGAGCAGAAGAGAGCCGAGCGC
Bio-rG4: WT MT
Input
Bead
KCl
LiCl
KCl
LiCl
HepAD38
Huh7
HepaRG
DDX5
DDX5
DDX5
B
DDX5: WT K144N D248N
HepaRG-DDX5-FLAG
FLAG
Bio-rG4: Input MT WT Input MT WT Input MT WT
protein intensity (Pulldown/Input)
1.5
1.0
0.5
0.0
ns
**
WT
K144N
D248N
C EMSA
WT K144N D248N
DDX5 (ng/µl) 0 1 10 100 100 0 1 10 100 100 0 1 10 100 100
Complex
Free RNA Oligos
Bio-rG4: WT MT WT MT WT MT

Figure 8

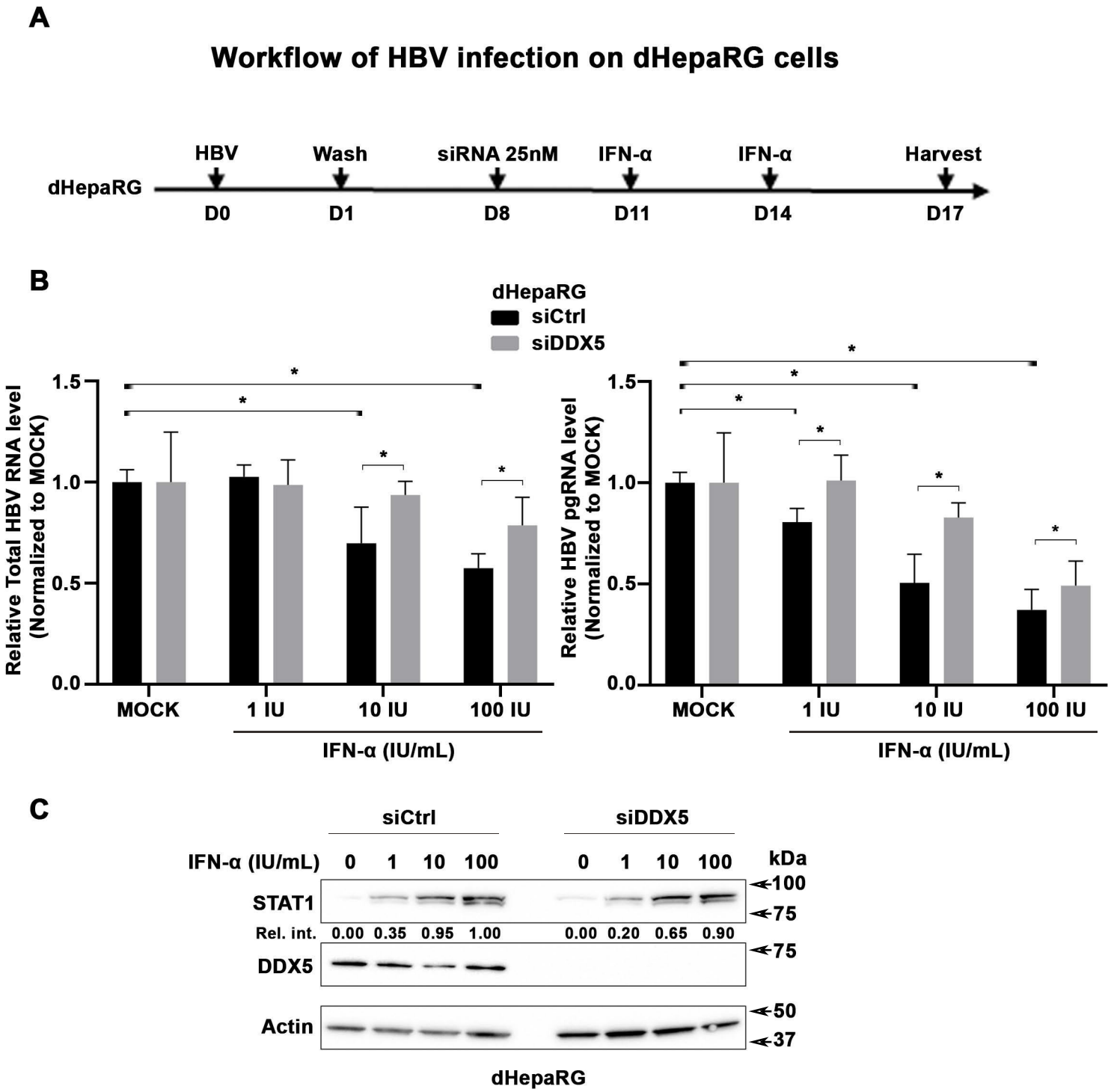
A
Workflow of HBV infection on dHepaRG cells
dHepaRG
HBV
Wash
siRNA 25nM
IFN-α
IFN-α
Harvest
D0
D1
D8
D11
D14
D17
B
dHepaRG
siCtrl
siDDX5
Relative Total HBV RNA level (Normalized to MOCK)
Relative HBV pgRNA level (Normalized to MOCK)
1.5
1.0
0.5
0.0
MOCK
1 IU
10 IU
100 IU
IFN-α (IU/mL)
C
siCtrl
siDDX5
IFN-α (IU/mL)
0
1
10
100
kDa
STAT1
100
75
Rel. int.
0.00
0.35
0.95
1.00
0.00
0.20
0.65
0.90
DDX5
75
Actin
50
37
dHepaRG

Figure 10

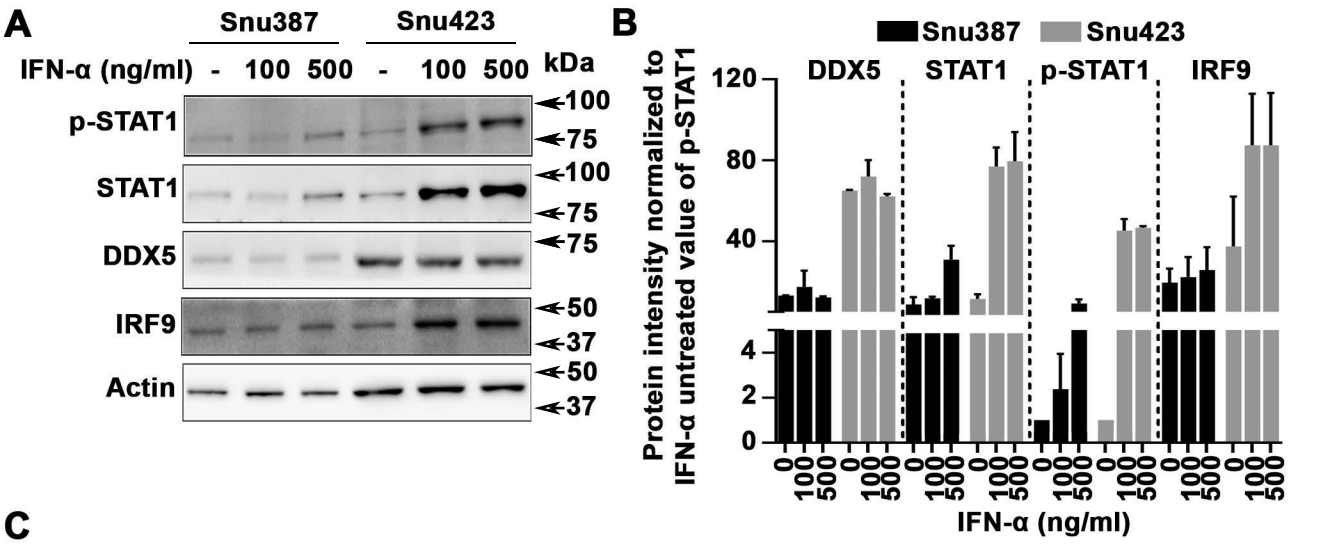

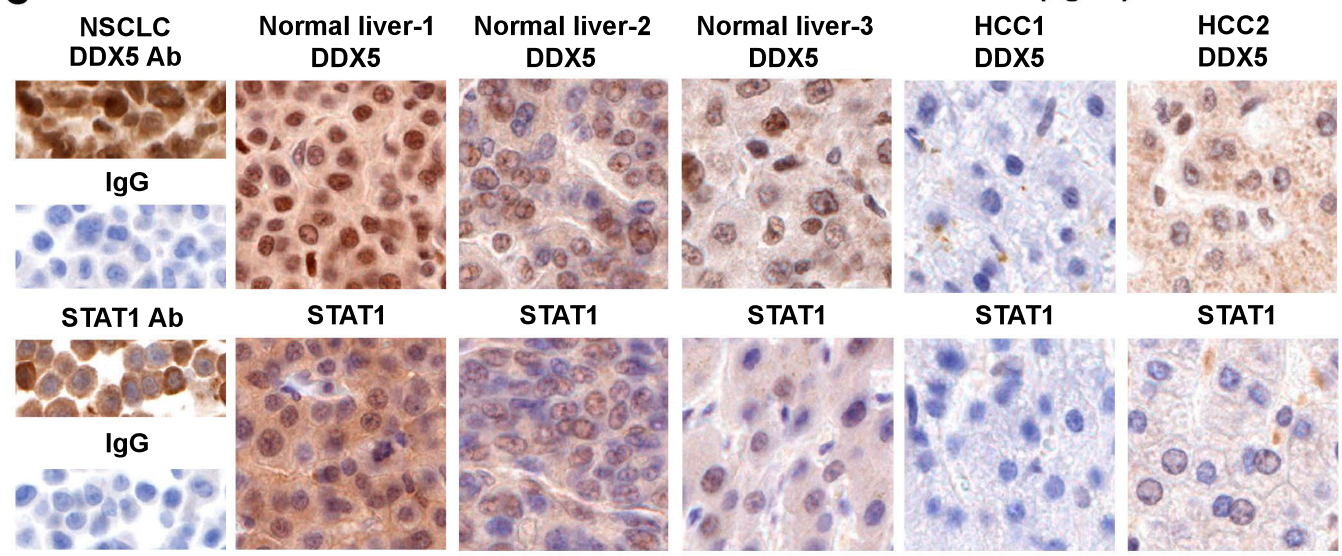

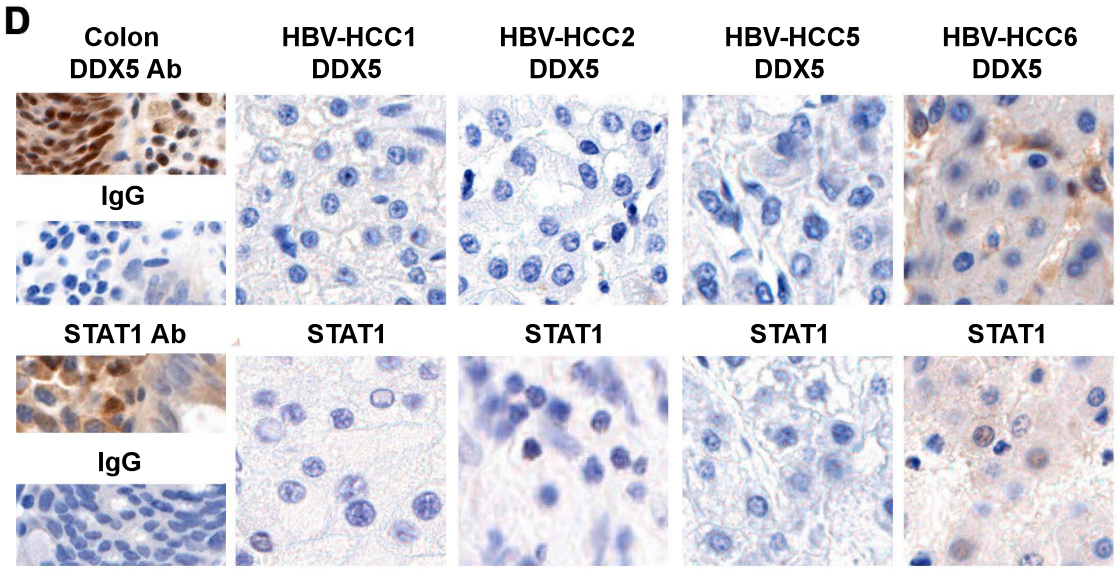

Case No.	HBV-HCC1	HBV-HCC2	HBV-HCC5	HBV-HCC6
Edmonson's grade	3	2/3	3	3

Figure 9

Supplementary information

RNA helicase DDX5 enables STAT1 mRNA translation and interferon signaling in hepatitis B virus replicating hepatocytes.

Jiazeng Sun[1,2], Guanhui Wu[2,3#], Florentin Pastor[4#], Naimur Rahman[1,2], Wen-Hung Wang[5], Zhengtao Zhang[6], Philippe Merle[7], Lijian Hui[6], Anna Salvetti[4], David Durantel[4], Danzhou Yang[2,3], and Ourania Andrisani[1,2*]

[1]Department of Basic Medical Sciences, [2]Purdue Center for Cancer Research, [3]Department of Medicinal Chemistry and Molecular Pharmacology, and [4] INSERM U1111-CNRS UMR5308 International Center for Infectiology Research (CIRI), [5]Gene Editing Core, Bindley Biosciences Center, Purdue University, West Lafayette, IN 47907. [6]Shanghai Institute of Biochemistry and Cell Biology, Chinese Academy of Sciences, Suzhou, Jiangsu 215121, China. [7]Department of Hepatology, Hôpital de la Croix-Rousse, Hospices Civils de Lyon, Université Lyon 1, Lyon, France

#equal contribution

*corresponding author: andrisao@purdue.edu

Department of Basic Medical Sciences,
Purdue University
201 S. University Street
West Lafayette, IN 47907-2064
Phone: 765-494-8131

Supplementary Figures

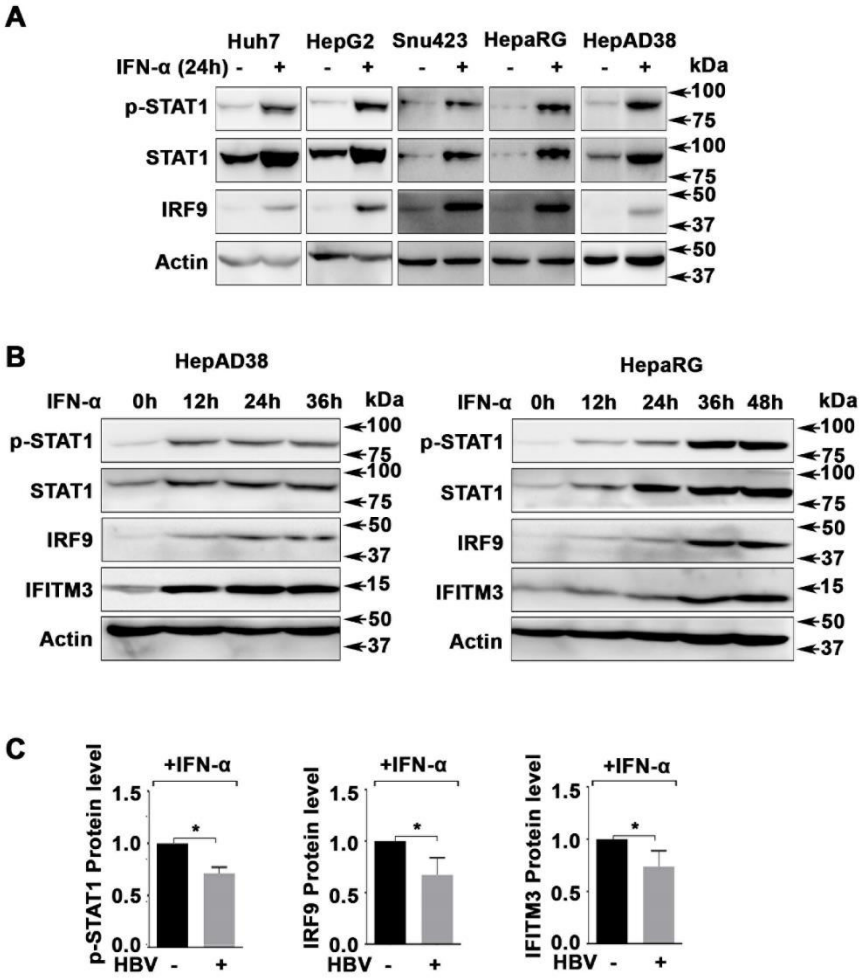

Figure S1

Figure S1. IFN-α response in various liver cancer cell lines. Immunoblots of IFN-α signaling related proteins using lysates from **(A)** Huh7, HepG2, Snu423, HepaRG and HepAD38 cells 24 h after IFN-α (500 ng/ml) treatment; **(B)** time course, 12-36 h of IFN-α (500 ng/ml) treatment in HepAD38 and HepaRG cells. **(C)** Quantification of indicated proteins from immunoblots in Figure 1A, using imageJ software**.**

Figure S2

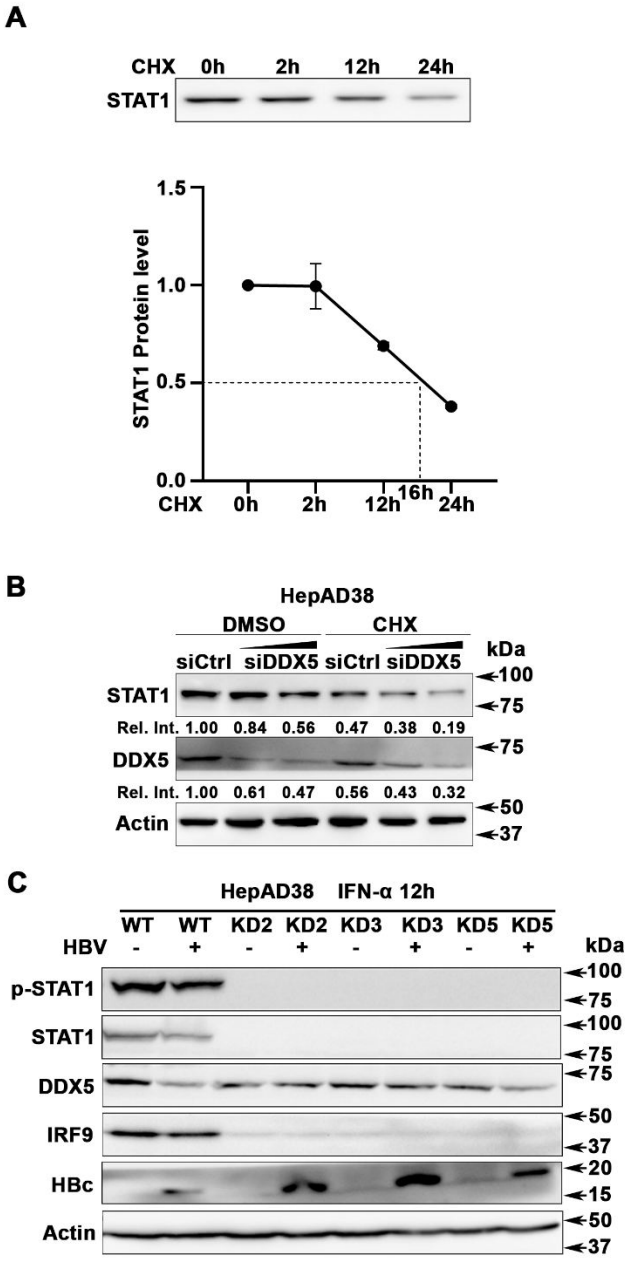

Figure S2. Quantification of t1/2 of STAT1 protein. (A) Immunoblot of STAT1 following treatment with 20 µg/ml cyclohexamide (CHX) for indicated time course in HepAD38 cells. Graph shows quantification of STAT1 t1/2. **(B)** Immunoblot of indicated proteins using lysates from HepAD38 treated or not with CHX **(**20 µg/ml) for 12h and transfected with siCtrl or increasing amount (20-40 nM) siDDX5 RNA. **(C)** Immunoblot of lysates from WT and KD2, KD3 and KD5 HepAD38 cells (1), treated with IFN-α for 12 h, +/- HBV replication for 3 days, for indicated proteins.

Figure S3

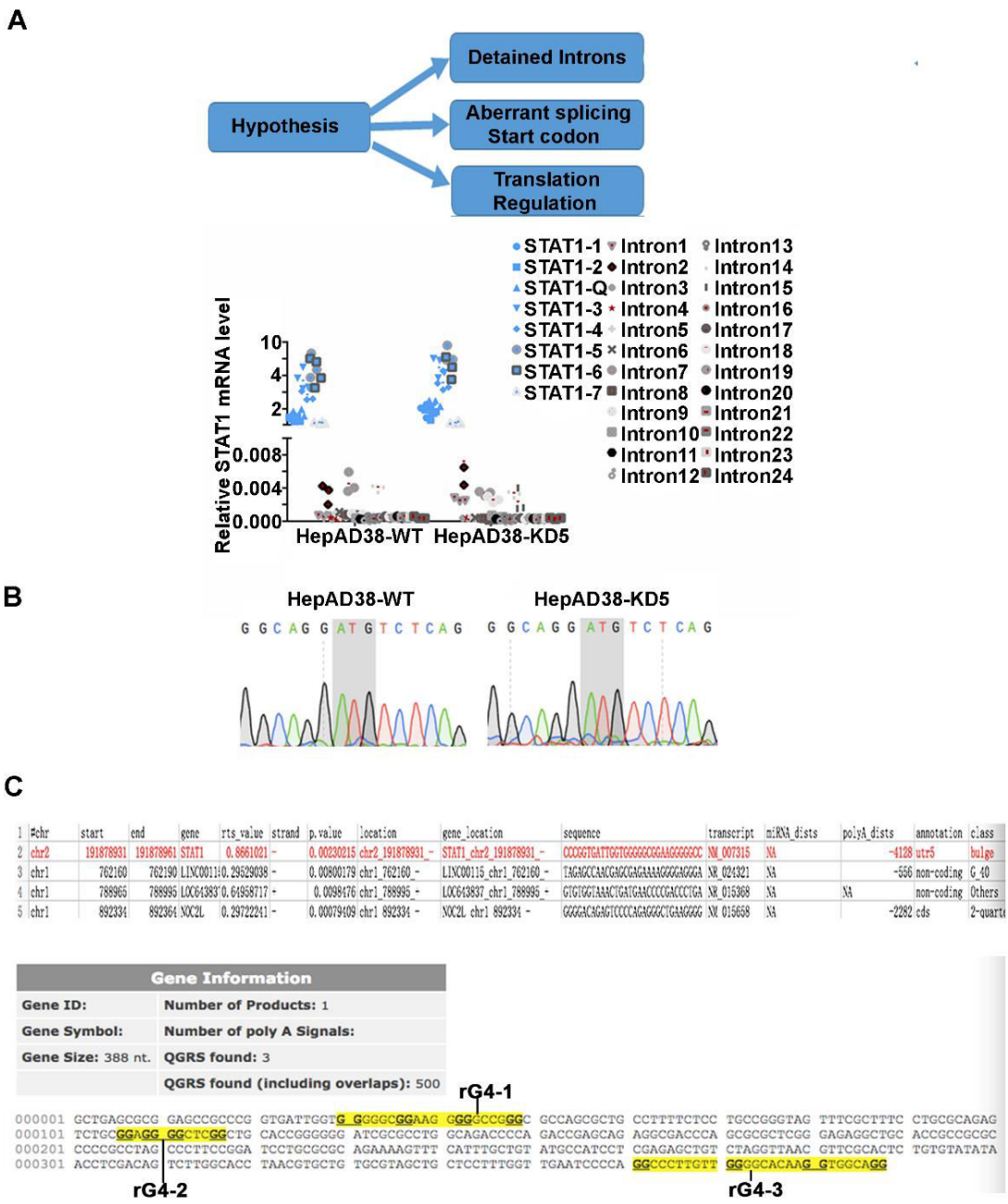

Figure S3. Mechanism of DDX5 effect on STAT1 regulation. (A) Diagram of post-transcriptional effects of DDX5 on STAT1 expression. QRT PCR quantifying expression of indicated exons (blue) and indicated introns (gray) in HepAD38-WT and HepAD38-KD5 (DDX5-knockdown) cell lines. N=3. Primer sequences are in Supplementary Table S3**. (B)** DNA sequencing of 5'UTR of STAT1 mRNA isolated from HepAD38-WT or HepAD38-KD5 cells. **(C).** Table listing the 5'UTR of STAT1 mRNA as containing a high probability G-quadruplex Structure (2)**.** Nucleotide sequence corresponding to the 5'UTR of human STAT1 mRNA. The highlighted sequences indicate the putative rG4 sequences.

Figure S4

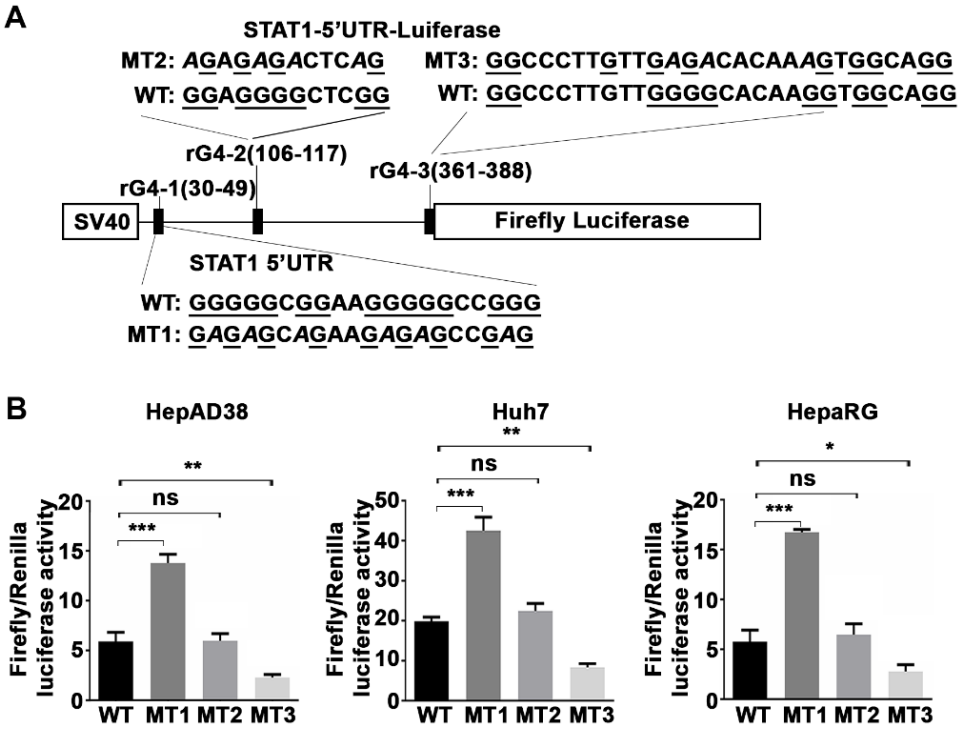

Figure S4. Putative rG4-2 and rG4-3 sequences of STAT1 5'UTR do not affect STAT1 translation. (A) Human STAT1 5'UTR upstream of Firefly (F.) Luciferase reporter, driven from the SV40 promoter. Putative rG4 sequences in 5' UTR indicated as rG4-1, rG4-2 and rG4-3. WT rG4-1 sequence is shown. Italics indicate site-directed changes in mutant MT1 of rG4-1, MT2 of rG4-2 and MT3, of rG4-3. **(B)** Ratio of Firefly/Renilla Luciferase activity at 24 h after co-transfection of WT or MT1, MT2 and MT3 STAT1-5'UTR-Luciferase and Renilla-Luciferase expression plasmids, in indicated cell lines. Statistical analysis from three independent biological replicates. *: $p<0.05$, **: $p<0.01$, ***: $p<0.001$, ns: not significant; Error bars indicate Mean ±SEM.

Figure S5

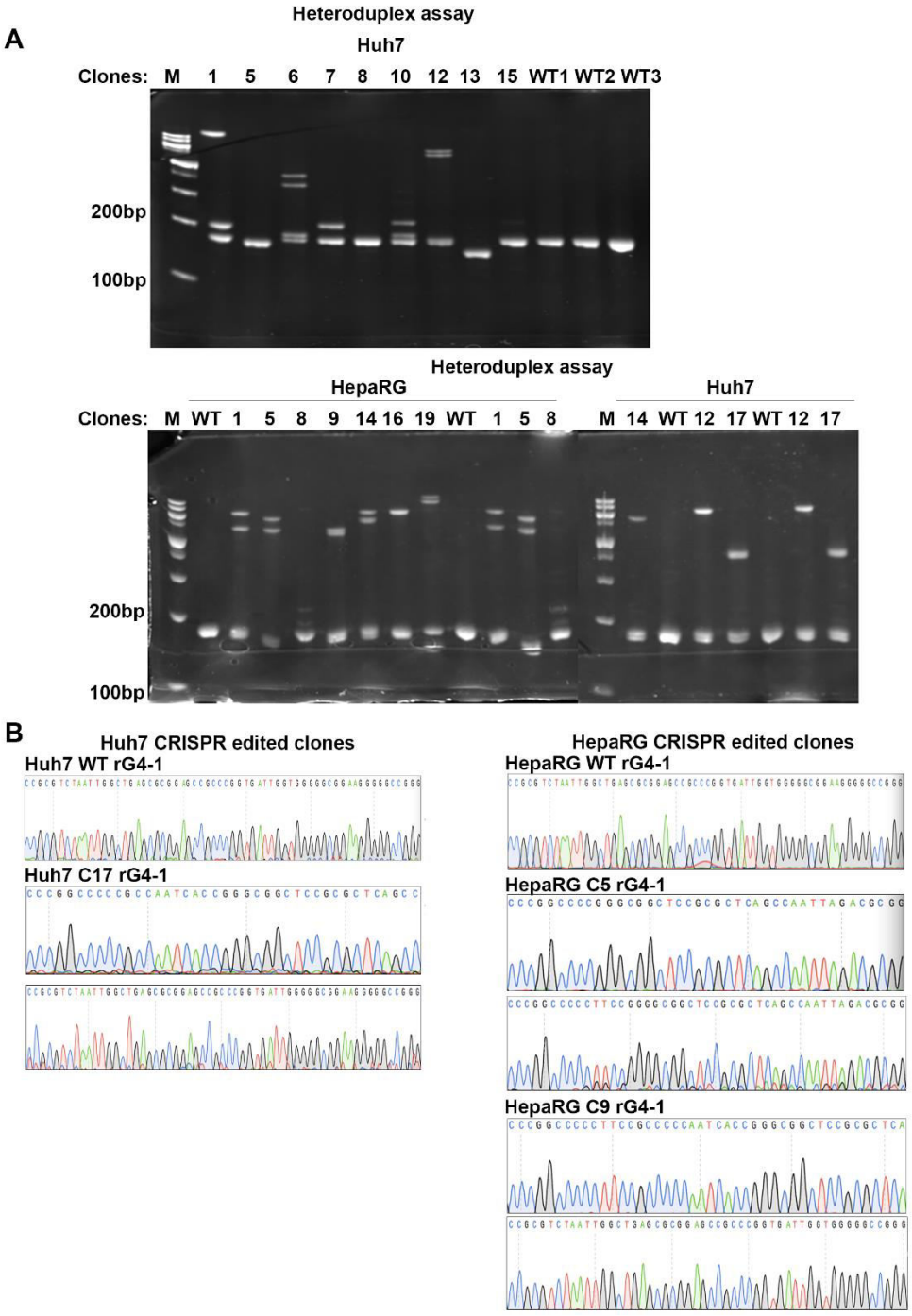

Figure S5. **Analyses of CRISPR/Cas9 edited cell lines: (A)** heteroduplex assay of various edited clones by agarose gel electrophoresis. **(B)** DNA sequence analyses of indicated edited clones.

Figure S6

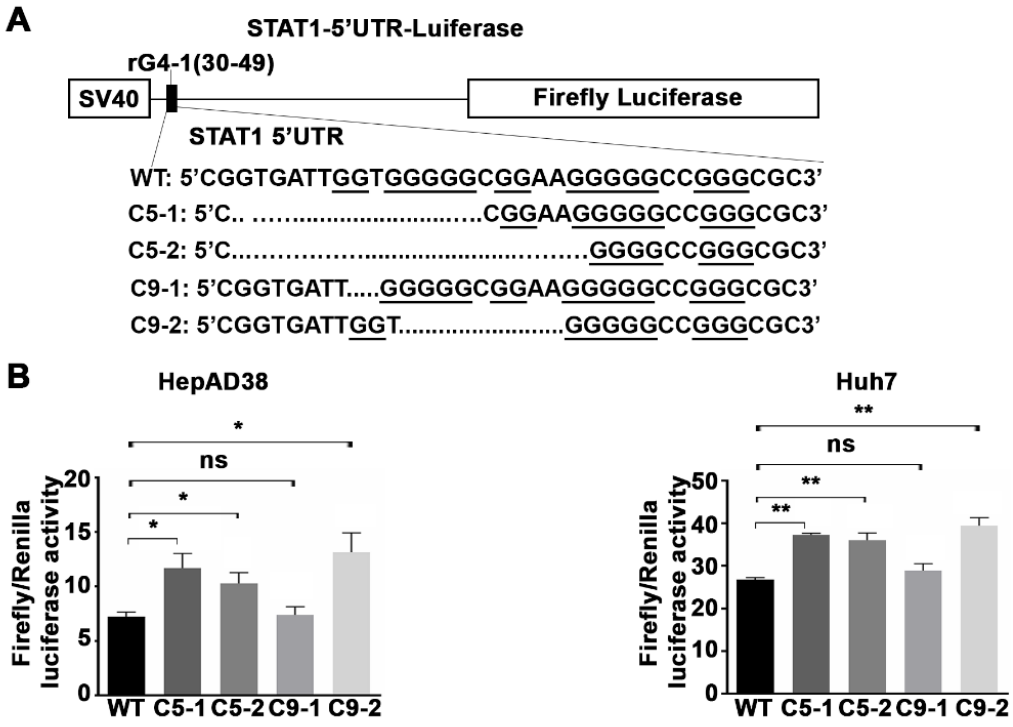

Figure S6. Activity of edited rG4-1 sequence studied by Luciferase reporter assays. (A) Sequence of edited rG4-1 sequences cloned into the indicated Luciferase expression vector. **(B) (B)** Ratio of Firefly/Renilla Luciferase activity at 24 h after co-transfection of WT and edited rG4-1 sequences in STAT1-5'UTR-Luciferase and Renilla-Luciferase expression plasmids, in indicated cell lines. Statistical analysis from three independent biological replicates. *: $p<0.05$, **: $p<0.01$, ***: $p<0.001$, ns: not significant; Error bars indicate Mean ±SEM.

Figure S7.

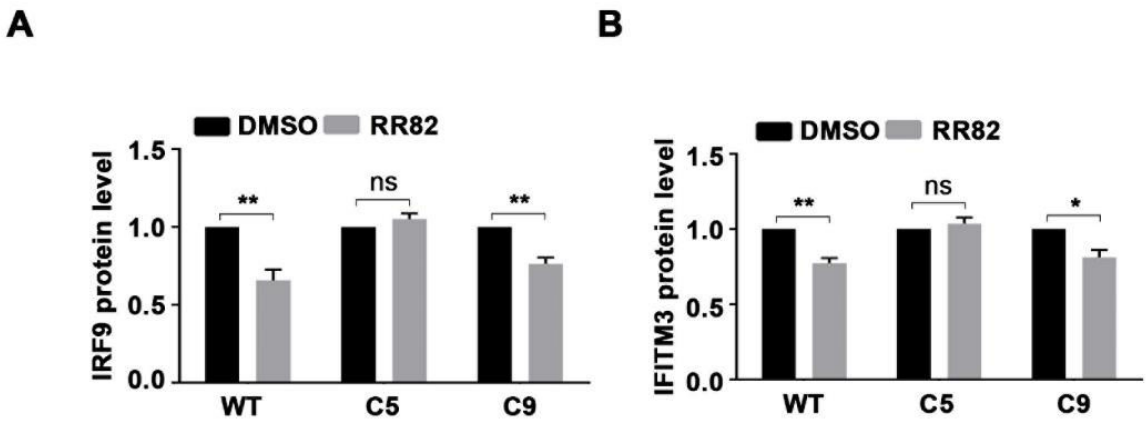

Figure S7. Quantification of immunoblots from Figure 5C using imageJ software. N=3

Figure S8

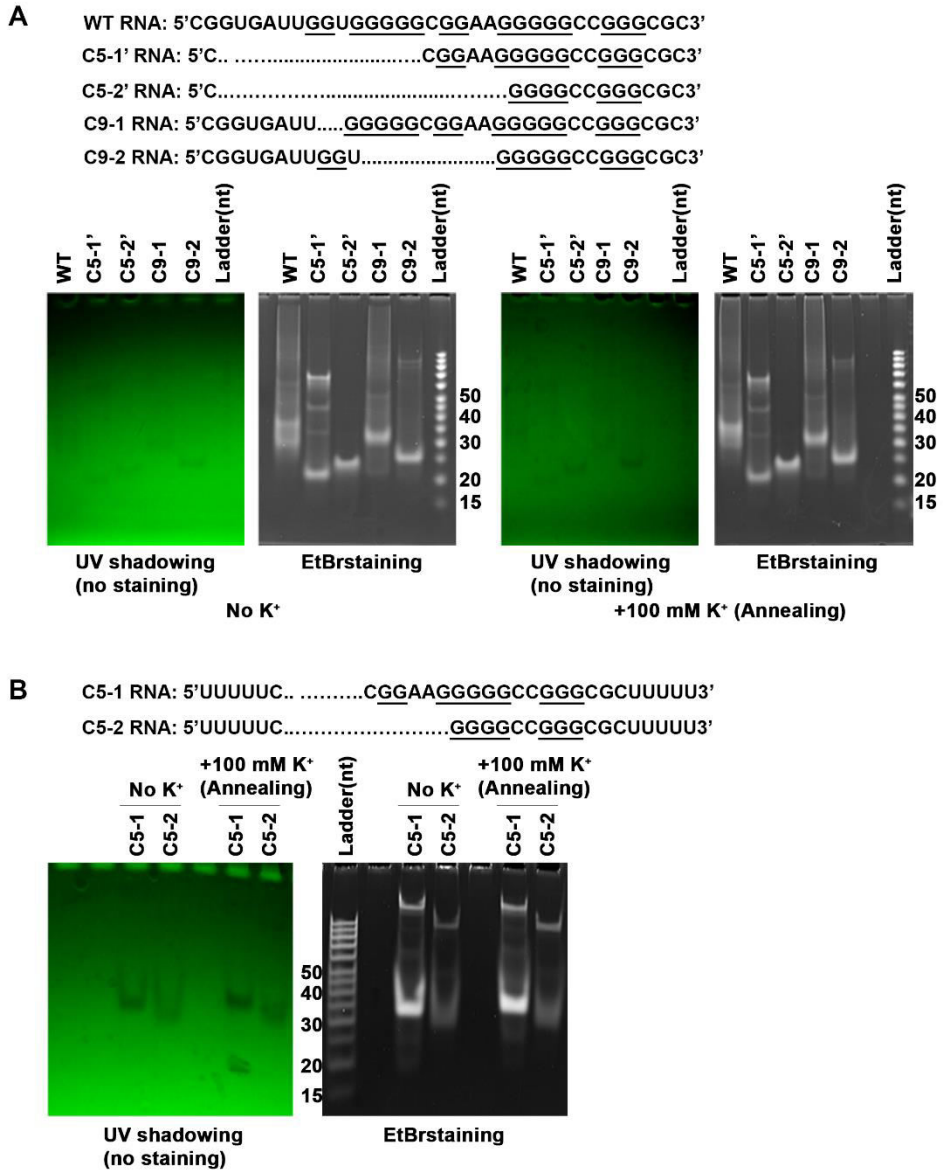

Figure S8. Analyses of synthesized RNA oligonucleotides shown in **(A and B)** by native agarose gel electrophoresis. Bands are the synthetic RNA oligonucleotides. MW markers are indicated.

Figure S9

A.

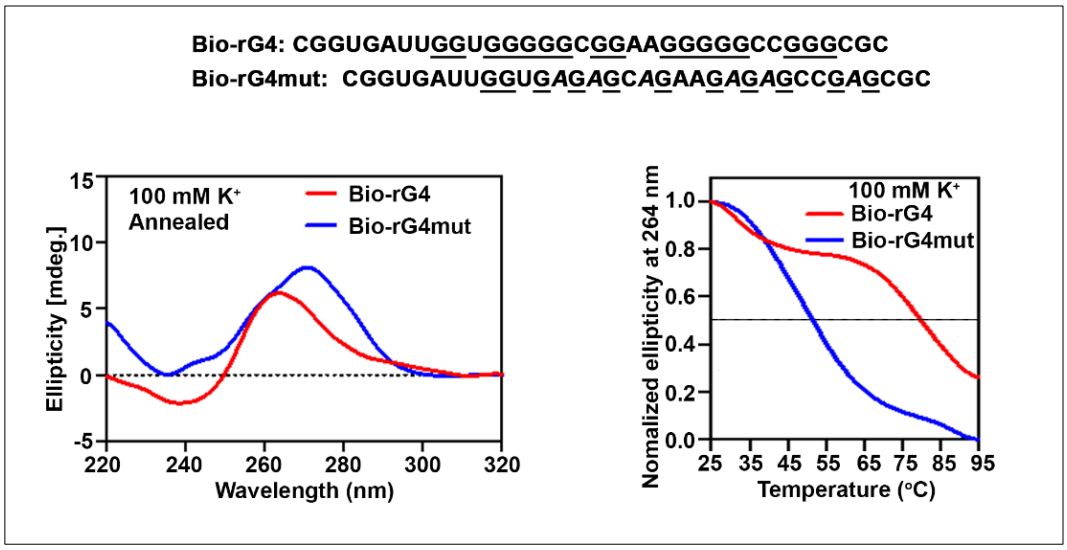

B.

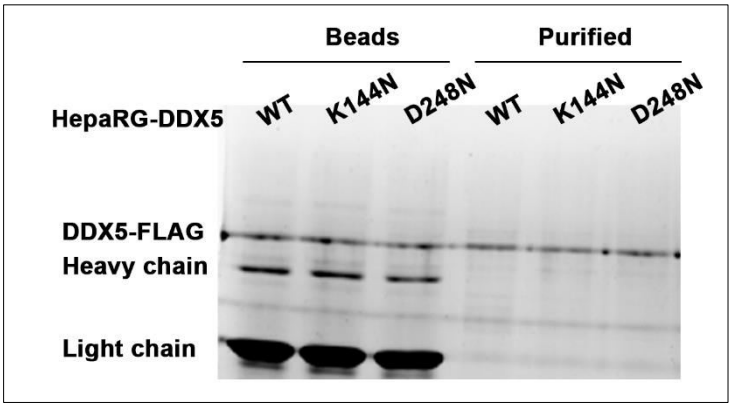

Figure S9. CD spectroscopy and melting curves of synthetic biotinylated RNA oligonucleotides used in pulldown assays. **A.** The sequence of bio-rG4 and bio-rG4mut of STAT1 is shown. Analyses included CD spectroscopy measurements (left panel) and melting curves (right panel). RNA oligonucleotides annealed by heating to 95°C and slowly cooled down to room temperature, in the presence of 100 mM K^+.

B. Immunoblot and PAGE detection of purified DDX5-FLAG proteins isolated from lysates prepared from HepaRG-DDX5-WT-FLAG, HepaRG-DDX5-K144N-FLAG and HepaRG-DDX5-D248N-FLAG expressing cells. Lysates were bound to FLAG-Antibody magnetic beads and DDX5-FLAG proteins were eluted by FLAG-M2 peptide, according to manufacturer's instructions.

Figure S10

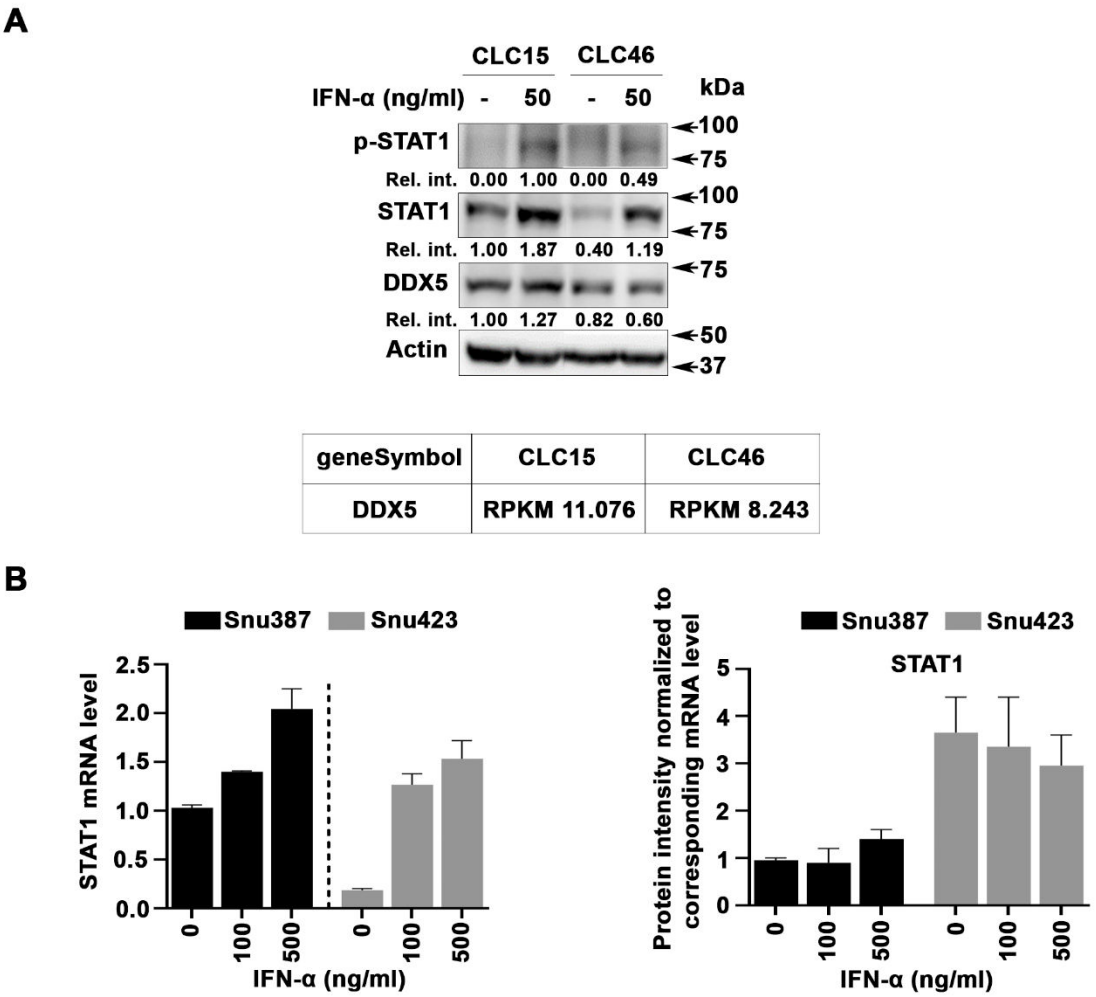

geneSymbol	CLC15	CLC46
DDX5	RPKM 11.076	RPKM 8.243

Figure S10A. Immunoblots using lysates of HBV-HCC derived cell lines (30) treated with IFN-α (50 ng/ml) for 12 h. Quantification by image J software is relative to actin. A representative assay is shown, n=2. The $\log_2$ RPKM values of DDX5 in CCL15 and CCL46 cell lines from the RNAseq studies (28) is shown.

B. (Left panel) Quantification by RT qPCR of STAT1 mRNA in Snu387 and 423 cell lines treated with IFN-α as indicated for 12 h. (Right panel) STAT1 protein from Fig. 9(A-B) normalized to STAT1 mRNA expressed in Snu387 *vs.* Snu423 cell lines, under the indicated treatment.

Figure S11

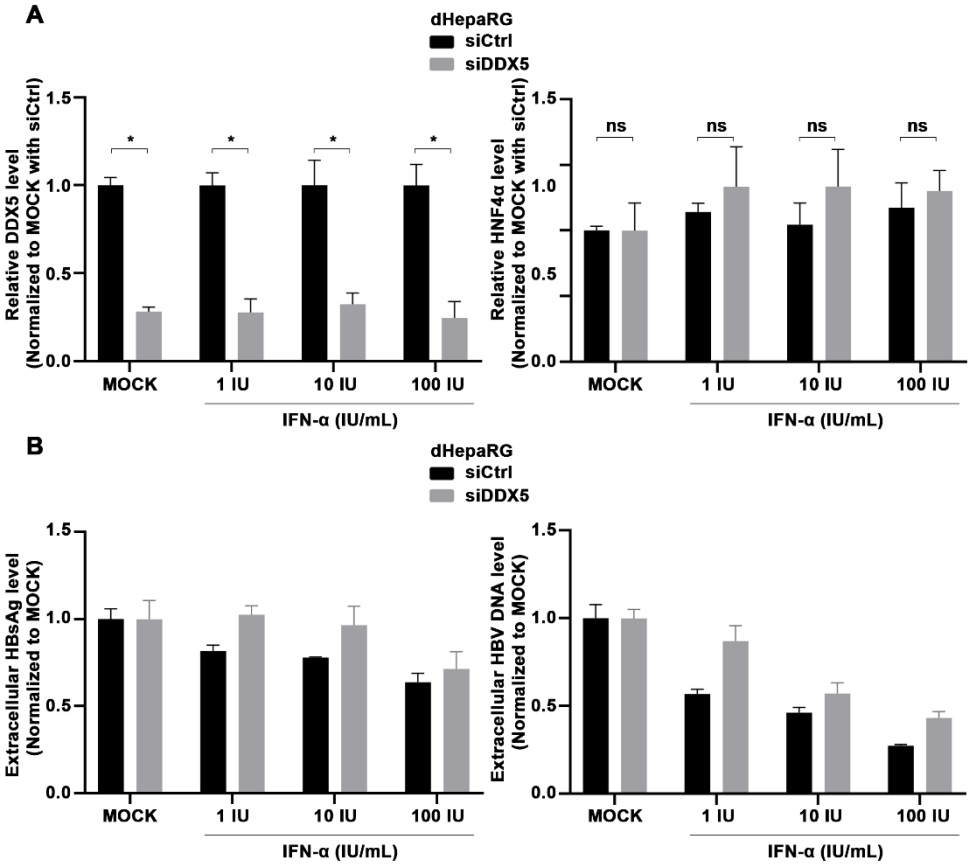

Figure S11. HBV infection in HepaRG cells. (A) qRT-PCR of indicated mRNAs using RNA isolated from HBV infected dHepaRG cells, as described in Fig. 10A, under conditions of IFN-α treated as indicated, in siCtrl vs. siDDX5 transfected cultures. **(B).** (Left panel) Supernatants isolated from HBV infected cells quantified by ELISA for HBsAg (Autobio kit); (Right panel) extracellular HBV DNA by qPCR. A representative experiment is shown (n=2)

Figure S12A

A

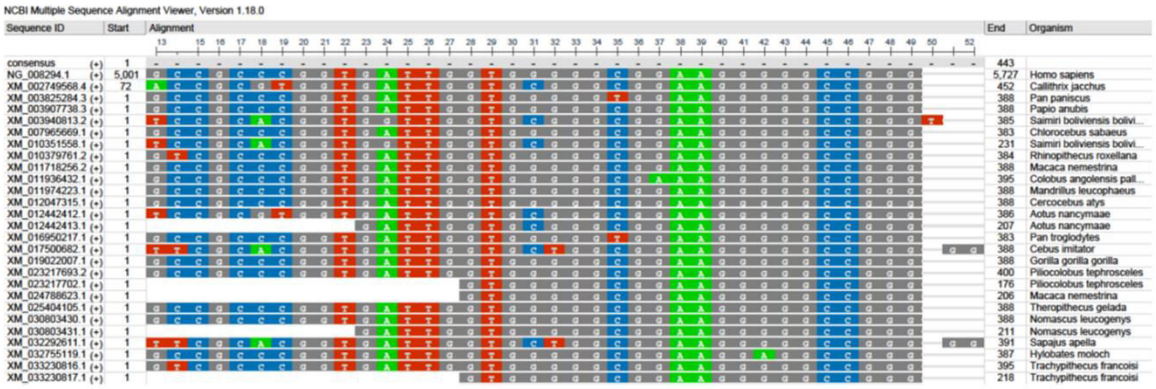

B

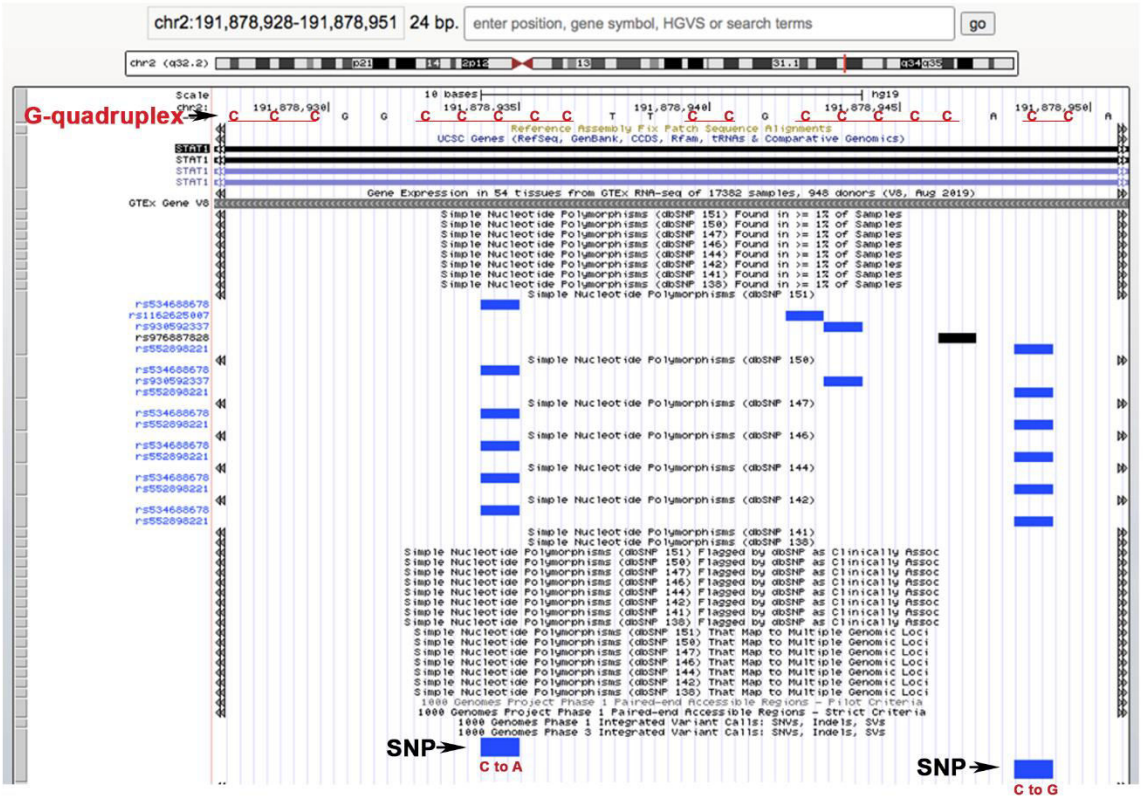

Figure S12: (A) Sequence alignment of the 5'UTR of STAT1 mRNA from indicated primates.

B. Identified SNPs that map in the rG4 sequence at the 5'UTR of STAT1.

Figure S13

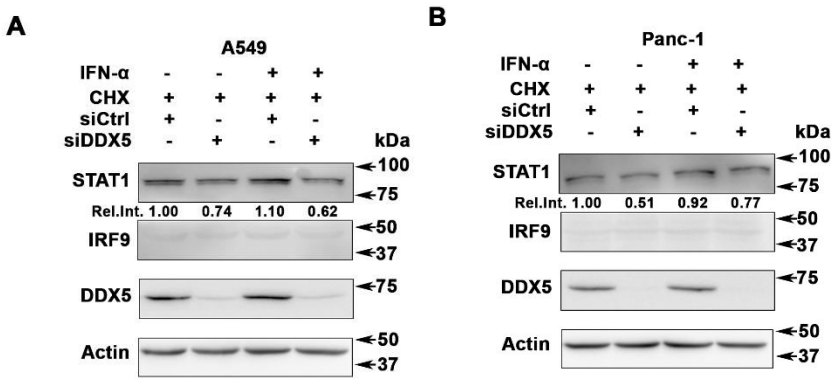

Figure S13. Immunoblots performed with indicated cell lines, examining effect of DDX5 knockdown on STAT1 protein levels. Interestingly, both cell lines tested lacked IFN-α responsiveness.

Supporting Table S1: List of Plasmids and siRNAs

Plasmids, siRNAs	Source
Wild Type (WT) STAT1-5'UTR-Luciferase	Addgene (#115353) (pFL-SV40-STAT1 5'-UTR was a gift from Ming-Chih Lai)
Mutant (MT)-STAT1-5'UTR-Luciferase	Constructed by site directed mutagenesis using the full-length WT 5'UTR as a template, and QuikChange II XL Site-Directed Mutagenesis kit (Agilent).
Renilla luciferase vector	Addgene (#27163)
PLVX	https://www.snapgene.com/resources/plasmid-files/?set=viral_expression_and_packaging_vectors&plasmid=pLVX-Puro
siCtrl	ThermoFisher Scientific (#4390843)
siDDX5-1	ThermoFisher Scientific (#4392420, assay id s4007)
siDDX5-2	ThermoFisher Scientific (#4392420, assay id s4008)
siSTAT1	ThermoFisher Scientific (#105153, assay id AM16708)

Supporting Table S2: Antibodies

Antibody	Dilution	Application	Source
Mouse α-Human p68	1:1000 in 2% BSA in TBST	Western Blot	Millipore Sigma (#05-850)
Rabbit α-Human STAT1	1:1000 in 2% BSA in TBST	Western Blot	Cell Signaling Technologies (#14994S)
Rabbit α-HBV Core	1:5000 in 2% BSA in TBST	Western Blot	Dr. Adam Zlotnick lab

Mouse α-Human Actin	1:1000 in 2% BSA in TBST	Western Blot	Sigma (#A5441)
Rabbit α-Human p-STAT1	1:1000 in 2% BSA in TBST	Western Blot	Millipore Sigma (#07-307)
Rabbit α-Human IRF9	1:1000 in 2% BSA in TBST	Western Blot	Cell Signaling Technologies (#76684S)
Rabbit α-Human IFITM3	1:1000 in 2% BSA in TBST	Western Blot	Cell Signaling Technologies (#59212S)
Rabbit α-Human NRAS	1:1000 in 2% BSA in TBST	Western Blot	Proteintech (#10724-1-AP)
Horse α-Mouse secondary	1:2000 in 2% BSA in TBST	Western Blot	Vector Laboratories (#PI-2000)
Goat α-Rabbit secondary	1:2000 in 2% BSA in TBST	Western Blot	Vector Laboratories (#PI-1000)
Rabbit α-Human DDX5	5 µg	RNA Immunoprecipitation	Cell Signaling Technologies (#9877S)
Rabbit IgG	5 µg	RNA Immunoprecipitation	Millipore Sigma (#17-700)
Rabbit α-Human DDX5	1:1000 in 2% BSA in TBST	Immunohistochemistry	Abacm (#ab205718)
Mouse FLAG	1:1000 in 2% BSA in TBST	Western Blot	Sigma (#F1804)
Mouse FLAG	5 µg	Ribonucleoprotein Immunoprecipitation	Sigma (#F1804)

Supporting Table S3: Primer and RNA oligonucleotide sequences

Primer	**5' – Sequence – 3'**
STAT1-Q-F	ATCAGGCTCAGTCGGGGAATA
STAT1-Q-R	TGGTCTCGTGTTCTCTGTTCT
DDX5-F	AGCAAGTGAGCGACCTTATC
DDX5-R	CATCCTTCATGCCTCCTCTAC
GAPDH-F	CCCTTCATTGACCTCAACTACA
GAPDH-R	ATGACAAGCTTCCCGTTCTC
Actin-F	GGCATGGGTCAGAAGGATT
Actin-R	GGGGTGTTGAAGGTCTCAAA
UBc-F	CCTGGAGGAGAAGAGGAAAGAGA
UBc-R	TTGAGGACCTCTGTGTATTTGTCA
HBV pgRNA-F	CTCCTCCAGCTTATAGACC
HBV pgRNA-R	GTGAGTGGGCCTACAAA
STAT1-1F	GCGCGCAGAAAAGTTTCATTTGC
STAT1-1R	CTGAGACATCCTGCCACCTTG
STAT1-2F	GTACGAACTTCAGCAGCTTGAC
STAT1-2R	GAAAATTATCCTGAAGATTACGC
STAT1-3F	AACGGAGGCGAACCTGAC
STAT1-3R	AACGGAGGCGAACCTGAC
STAT1-4F	AGAGCCAATGGAACTTGATGG
STAT1-4R	ACTATCCGAGACACCTCGTC
STAT1-5F	TCCTGCTACTCTGTTCCTTCAC
STAT1-5R	CCCTCATTCTCGTCCTGATAC
STAT1-6F	CTGCTTTCATCTTGGTCACATAC
STAT1-6R	AAAGTAGCCCATTTAAGAAACATG

STAT1-7F	ATGGCGAGAACCTAAGTTTCAG
STAT1-7R	GCAGTAAAATGAAACCATGCCG
Intron-1F	GCGCGCAGAGTGAGTGGCCG
Intron-1R	TGGAATACTCAGGACGCGTTC
Intron-2F	CAAGGTGGCAGGTCAGTAAATG
Intron-2R	GAACTCTTCAGTACCGGCCAG
Intron-3F	CAAGACTGGTAAGGAAAATTCAC
Intron-3R	GTTGAGACACTTTTTGGCTCAAC
Intron-4F	CGTAATCTTCAGGTATGACCTGG
Intron-4R	ATGCTATATTTACTGATGCTGTAG
Intron-5F	AATCAGGTACTTTTTTCTCATTG
Intron-5R	CTCTAAATCTGATTCTCCCACTTC
Intron-6F	CAAGGTTATGGTGAGTATTGAG
Intron-6R	ACTTATAGCTTGAGACTTCTGC
Intron-7F	AGAACAGAGGTAAGGGTTCAC
Intron-7R	TGGCCTGGGTTATCAAGGAAG
Intron-8F	GAGAAAGGTAGTTATTTACTTTCC
Intron-8R	TTTCATTCTCAACTGGGGCTC
Intron-9F	GAACTGGTAAGATTCTCCAAAGC
Intron-9R	CTGTGCTTTCCAAGGGAGTG
Intron-10F	ATTCAGAGGTAACTCAAGGGAC
Intron-10R	CCTGGGTGATAGGTGAGACTC
Intron-11F	GTTGAGGTAACAAGGGAAAGATG
Intron-11R	CTCTCAGATATTCTCAGTAAGAG
Intron-12F	ATTTGATAAGTAAGATATCTTTAAC
Intron-12R	GGCAAACTTCCACCCAGTATAG

Intron-13F	ACAGTAAAAGGGTACGTGACG
Intron-13R	CTATACAATATAGGAAAGAAATGC
Intron-14F	GGCACCTGGTAGGGACATCA
Intron-14R	AGTACTGGCGACAGGAAGAC
Intron-15F	CCAGAACGAATGAGGTGAGAG
Intron-15R	GTGGTGTTTTTACTGTTGTCACAG
Intron-16F	GGTAATTGACCTCGAGGTAAGAC
Intron-16R	CAATTGTCTAGCTTTCTGGACCA
Intron-17F	AACCCAGGGTATGGAAAACAC
Intron-17R	ATATCCATGCTTCATATTCCCAG
Intron-18F	GAGAGAAGCTTCTTGGTATATGC
Intron-18R	GTGACATATGATTCTCACTTAGC
Intron-19F	GGTTTTGTAAGGTGAGGACTG
Intron-19R	AATGTTATCACTCAGGCAGGTG
Intron-20F	GGAATGATGGGTAAGGGCCA
Intron-20R	GTTCTACTCTTCTGAAGCCCTG
Intron-21F	AGGCGGTGAGTGGGAGTTTG
Intron-21R	AGAGAGTGAACCACAACCAC
Intron-22F	TCCAGGCCAAAGGAAGGTAAG
Intron-22R	GCTGTATCAGGCCAAATAATGC
Intron-23F	GTGTCTGAAGTGTAAGTGAACAC
Intron-23R	AAATGCTGATAGGCAGTAACAC
Intron-24F	CGACAGTATGGTGAGTACCAC
Intron-24R	AGGTGGTTTAAATCCAGCAGC
Fluc-F	CTCACTGAGACTACATCAGC
Fluc-R	TCCAGATCCACAACCTTCGC

Rluc-F	GGAATTATAATGCTTATCTACGTGC
Rluc-R	CTTGCGAAAAATGAAGACCTTTTAC
STAT1-F 5'UTR EcoRI	CGGAATTCGCTGAGCGCGGAGCCGCCCGG
Stat1-F 5'UTR NcoI	CATGCCATGGCCTGCCACCTTGTGCCCCAAC
MT1-F	CCGGTGATTGGTGAGAGCAGAAGAGAGCCGAGCGCCAGCGCTGC
MT1-R	GCAGCGCTGGCGCTCGGCTCTCTTCTGCTCTCACCAATCACCGG
MT2-F	GCGCAGAGTCTGCAGAGAGACTCAGCTGCACCGGGGGG
MT2-R	CCCCCGGTGCAGCTGAGTCTCTCTGCAGACTCTGCGC
MT3-F	GAATCCCCAGGCCCTTGTTGAGACACAAAGTGGCAGGCCATGGAAGACG
MT3-R	CGTCTTCCATGGCCTGCCACTTTGTGTCTCAACAAGGGCCTGGGGATTC
MT-C5-1-F	GCTGAGCGCGGAGCCGCCCCGGAAGGGGGCCGGGCGCCA
MT-C5-1-R	TGGCGCCCGGCCCCCTTCCGGGGCGGCTCCGCGCTCAGC
MT-C5-2-F	GCTGAGCGCGGAGCCGCCCGGGGCCGGGCGCCAGCGCTG
MT-C5-2-R	CAGCGCTGGCGCCCGGCCCCGGGCGGCTCCGCGCTCAGC
MT-C9-1-F	CGCGGAGCCGCCCGGTGATTGGGGGCGGAAGGGGGCCGGG
MT-C9-1-R	CCCGGCCCCCTTCCGCCCCCAATCACCGGGCGGCTCCGCG
MT-C9-2-F	GGAGCCGCCCGGTGATTGGTGGGGGCCGGGCGCCAGCGC
MT-C9-2-R	GCGCTGGCGCCCGGCCCCCACCAATCACCGGGCGGCTCC
STAT1-seq-F	TGTATGCCATCCTCGAGAGC
STAT1-seq-R	CAGTCTTGCTTTTCTAACCACTG
SV40-F	TATTTATGCAGAGGCCGAGG
M13-R	CAGGAAACAGCTATGAC
CRISPR-seq-F	AAGCCGGCGGAAATACCC
CRISPR-seq-R	TCTGCTCGGTCTGGGGTC

CRISPR-heter-F	GGAAGCCGGCGGAAATAC
CRISPR-heter-R	GCGCAGGAAAGCGAAACTA
CRISPR-gRNA1	rArGrCrCrGrCrCrCrGrGrUrGrArUrUrGrGrUrGrG
CRISPR-gRNA2	rCrGrGrUrGrArUrUrGrGrUrGrGrGrGrCrGrGrA
WT (rG4-1) RNA oligos	rCrGrGrUrGrArUrUrGrGrUrGrGrGrGrCrGrGrArArGrGrGrGrCrCrG rGrGrCrGrC
C5-1 RNA oligos	rUrUrUrUrUrCrCrGrGrArArGrGrGrGrCrCrGrGrGrCrGrCrUrUrUrUrU
C5-2 RNA oligos	rUrUrUrUrUrCrGrGrGrGrCrCrGrGrGrCrGrCrUrUrUrUrU
C9-1 RNA oligos	rCrGrGrUrGrArUrUrGrGrGrGrGrCrGrGrArArGrGrGrGrGrCrCrGrGrGrC rGrC
C9-2 RNA oligos	rCrGrGrUrGrArUrUrGrGrUrGrGrGrGrCrCrGrGrGrCrGrC
C5-1’ RNA oligos	rCrCrGrGrArArGrGrGrGrGrCrCrGrGrGrCrGrC
C5-2’ RNA oligos	rCrGrGrGrGrCrCrGrGrGrCrGrC
Bio-rG4 RNA oligos	rCrGrGrUrGrArUrUrGrGrUrGrGrGrGrCrGrGrArArGrGrGrGrCrCrG rGrGrCrGrC
Bio-rG4mut RNA oligos	rCrGrGrUrGrArUrUrGrGrUrGrArGrArGrCrArGrArArGrArGrArGrCrCrG rArGrCrGrC

Supporting Table S4: Reagents, Chemical inhibitors, and Kits

Reagents, Chemical inhibitors, Kits	**Source**
Cycloheximide (CHX)	Cell Signaling Technologies (#2112)
IFN-α	Millipore Sigma (#SRP4596)
RR82	ChemSpider (324571151)
PhenDC3	Polysciences (#26000-1)
TMPyP2	Dr. Danzhou Yang
TMPyP4	Dr. Danzhou Yang
PCR Mycoplasma Detection Kit	Abm (#G238)
Dual-Luciferase® Reporter Assay System	Promega (#1980)
Cell Lysis Buffer (10X)	Cell Signaling Technology (#9803)
LightCycler® 480 SYBR Green I Master	Roche (#04887352001)
iScript™ cDNA Synthesis Kit	Biorad (#1708891)
Nitrocellulose Membrane, Roll, 0.2 µm	Biorad (#1620112)
LightCycler® 480 Sealing Foil	Roche (#04729757001)
LightCycler® 8-Tube Strips (white)	Roche (#06612601001)
DMSO	Sigma (#D8418-50ML)
Tween™ 20	ThermoFisher Scientific (BP337-500)
Tetracycline hydrochloride	Sigma (#T7660-5G)
Bovine Serum Albumin	Sigma (#A9647-100G)
Pierce™ ECL Western Blotting Substrate	ThermoFisher Scientific (#32106)
Geneticin™ Selective Antibiotic (G418 Sulfate)	ThermoFisher Scientific (#10131027)
Pierce™ BCA Protein Assay Kit	ThermoFisher Scientific (#23227)
Lipofectamine™ 3000 Transfection Reagent	ThermoFisher Scientific (#L3000015)
Lipofectamine™ RNAiMAX Transfection Reagent	ThermoFisher Scientific (#13778150)

Restore™ PLUS Western Blot Stripping Buffer	ThermoFisher Scientific (#46430)
RNeasy Mini Kit	Qiagen (#74104)
Magna RIP™ RNA-Binding Protein Immunoprecipitation Kit	Millipore Sigma (#17-700)
CRISPRevolution sgRNA EZ Kit	SYNTHEGO
QuikChange II XL Site-Directed Mutagenesis Kit	Agilent (#200521)
Streptavidin MagneSphere Paramagnetic Particles	Promega (#Z5481)
Glycerol	Promega (#H5433)
KCl (2M), RNase-free	Fisher Scientific (AM9640G)
LiCl Precipitation Solution (7.5 M)	Fisher Scientific (AM9480)
RIPA Lysis and Extraction Buffer	Fisher Scientific (89900)
Anti-FLAG M2 Magnetic Beads	Millipore Sigma (#8823)
3XFLAG peptide	Millipore Sigma (#F4799)
SYBR^{TM}-Gold dye	ThermoFisher Scientific (#S11494)

References

1. Mani SKK, Yan B, Cui Z, Sun J, Utturkar S, Foca A, Fares N, et al. Restoration of RNA helicase DDX5 suppresses hepatitis B virus (HBV) biosynthesis and Wnt signaling in HBV-related hepatocellular carcinoma. Theranostics 2020;10:10957-10972.
2. Kwok CK, Marsico G, Sahakyan AB, Chambers VS, Balasubramanian S. rG4-seq reveals widespread formation of G-quadruplex structures in the human transcriptome. Nat Methods 2016;13:841-844.